Variational multiparticle-multihole configuration mixing method applied to pairing correlations in nuclei

N. Pillet,[1] J.-F. Berger,[1] and E. Caurier[2]

[1]*CEA, DPTA, Service de Physique Nucléaire, Bruyères-le-Châtel, F-91297 Arpajon, France*

[2]*Département Recherches Subatomiques, Institut Pluridisciplinaire Hubert Curien, 23 rue du Loess, BP28, F-67037 Strasbourg, France*

(Received 16 June 2008; published 12 August 2008)

Applying a variational multiparticle-multihole configuration mixing method whose purpose is to include correlations beyond the mean field in a unified way without particle number and Pauli principle violations, we investigate pairing-like correlations in the ground states of ^{116}Sn, ^{106}Sn, and ^{100}Sn. The same effective nucleon-nucleon interaction, namely, the D1S parametrization of the Gogny force, is used to derive both the mean field and correlation components of nuclear wave functions. Calculations are performed using an axially symmetric representation. The structure of correlated wave functions, their convergence with respect to the number of particle-hole excitations, and the influence of correlations on single-particle level spectra and occupation probabilities are analyzed and compared with results obtained with the same two-body effective interaction from BCS, Hartree-Fock-Bogoliubov, and particle number projected after variation BCS approaches. Calculations of nuclear radii and the first theoretical excited 0^+ states are compared with experimental data.

DOI: 10.1103/PhysRevC.78.024305 PACS number(s): 21.60.Jz, 21.30.Fe, 27.60.+j

I. INTRODUCTION

Microscopic approaches based on the self-consistent mean-field theory and its extensions are among the most powerful methods of describing many-body interacting systems. These approaches have been used for many years in nuclear physics [1] as well as in atomic and molecular physics [2,3]. In nuclear physics, they are usually based on energy density functionals built from phenomenological parametrizations of the nucleon-nucleon effective interaction as the Skyrme forces [4,5] or the Gogny interaction [6].

In nuclei away from closed shells, pairing correlations are known to play a very important role. The techniques commonly used to describe them in a microscopic framework are the Hartree-Fock (HF) + BCS and Hartree-Fock-Bogoliubov (HFB) approaches. Whereas these approaches have proved to provide an excellent description of observables associated with pairing such as gaps or odd-even mass differences in superfluid nuclei, they suffer from the defect that pairing correlations are introduced by means of a wave function –the BCS wave function —that does not represent a definite number of nucleons. As a consequence, strongly paired nuclear states contain spurious nucleon number fluctuations that may be large. In addition, those correlations induced by the nuclear pairing interaction are not described in weakly correlated regimes [7,8].

This problem, which arises from the particular form of the BCS wave function, has led to a revival of the study of pairing correlations in atomic nuclei in the last five years. Namely, methods have been implemented by several groups based on particle number projected BCS wave functions [9–13]. Whereas projection of the self-consistent HFB or BCS wave functions—the projection after variation (PAV) technique—allows one to restore nucleon numbers and to compute the corresponding correction to the total binding energy, only the variation after projection (VAP) procedure, either in the form of the approximate Lipkin-Nogami technique or using the exact formalism, is able to describe correlations in situations where BCS or HFB pairing is small. It is shown in Ref. [13] that the two kinds of approach lead to significant differences in the correlation content of projected wave functions.

In this work, we envisage an alternative to these projection methods by applying a variational multiparticle-multihole (mp-mh) configuration mixing technique. This approach is similar to the multiconfiguration Hartree-Fock method (MCHF) [2] well-known in atomic physics or to the multiconfiguration self-consistent field method (MCSCF) [3] employed in molecular physics, and it can be used to describe not only pairing correlations but also other kinds of long-range correlations such as those associated with collective vibrations. The wave function of the system is assumed to be a superposition of a finite set of Slater determinants which includes a HF-type state together with multiple particle-hole (p-h) excitations of this state. Both the configuration mixing coefficients and the single-particle states are determined in a self-consistent way from a variational procedure.

Let us emphasize that, contrary to the wave functions used in the large-scale shell model approach [14,15], p-h excitations are not restricted to those within one major shell. They are built from the full (finite) single-particle spectrum obtained in the HF-like calculation. On the other hand, only excited configurations involving a relatively small number of p-h excitations have to be taken into account. This is because single-particle states are derived from a self-consistent mean field that already contains a large part of the effect of two-body interactions. It has been shown in Ref. [16] that pairing correlations in usual superfluid nuclei can be accurately described using excitations involving the excitation of no more than three conjugate pairs of like nucleons.

One important advantage of such an approach is to describe correlations in a formalism that explicitly preserves particle number conservation and never violates the Pauli principle (contrary to, e.g., random-phase approximation

(RPA) correlations). In the case of pairing, as will be seen in Sec. II, the mp-mh method is more general than the fully VAP procedure. It is therefore in position to describe both strong pairing correlations without particle number violation as well as the particular correlations occurring in weakly paired systems.

Pioneering work along this line in nuclear physics has used an approach referred to as the Higher Tamm-Dancoff approximation (HTDA) [17]. In this kind of approach, the nuclear mean field that provides the single-particle states is derived from an energy density functional built with an effective force of the Skyrme family, and correlations are generated by means of a simplified phenomenological residual interaction in the form of a contact two-body force. This method has been used to describe the behavior of nuclei as a function of quadrupole deformation and the properties of long-lived nuclear states such as isomeric states in the ^{178}Hf nucleus. Extensions of this work, where the residual interaction is treated in a perturbative way, in the spirit of a highly truncated shell model, can be found in Ref. [18]. An attempt in this direction was previously proposed in Ref. [19]. Let us also mention a similar approach proposed in Ref. [20] to describe pairing correlations in a fully particle-number conserving way.

In the present mp-mh configuration mixing approach, the ground state and first excited states are derived variationally from an energy density functional taken as the mean-value within the mp-mh wave function of the effective Hamiltonian built with the Gogny force. Calculations are performed using an axially symetric representation of single-particle states. The density distribution entering the density-dependent term of the Gogny force has been taken as the one built from the correlated mp-mh wave function. This prescription has been adopted in the VAP onto the particle number procedure [9–11], in the context of the projected HFB approach. Although there is no justification for using this correlated density distribution in the effective force, such a choice has been made in order to naturally obtain in the variational procedure the so-called rearrangement terms that are known to play a crucial role in the matrix elements of the mean field [6] and also of the residual interaction. The importance of including such rearrangement terms is clearly exposed and illustrated in Refs. [21–24] in the context of RPA and QRPA methods. Let us mention that the use of a unique effective two-body interaction for deriving in a unified way both the single-particle structure associated with the nuclear mean field and the correlations beyond the mean field is clearly an advantage in the context of a completely microscopic description of nuclear states. It reduces the phenomenological part of the present nuclear structure approach, as the only parameters are those of the nucleon-nucleon effective interaction.

In the present work, we will only study correlations of the pairing type, leaving for further work other kinds of correlations. The mp-mh trial wave function will therefore be restricted to a superposition of configurations taken as BCS-type pair excitations. Here, a BCS-type pair is defined as two protons or two neutrons in time-reversed states. By making this choice, only the usual pairing part of the residual interaction—the singlet even component—is taken into account in the description of correlations. In particular, proton-neutron pairing-type correlations are not taken into account in the present study.

The aim of the present work is to analyze pairing-type correlations in nuclei in three different situations: large BCS pairing, medium BCS pairing, and no BCS pairing by analyzing three well-known nuclei: ^{116}Sn, ^{106}Sn, and ^{100}Sn. The quantities that will be examined are the total correlation energy, the structure of the correlated ground state wave function, particularly the respective weights of the HF-type wave function and of the different mp-mh pair excitations, and the influence of correlations on single-particle energies and occupation probabilities. Comparisons will be made with the usual HFB results derived from the same Gogny two-body effective interaction and with those of projection methods such as projected BCS (PBCS) after variation. Nuclear radii and the energy and structure of the first theoretical excited 0^+ state will be compared with experimental data.

The paper is organized as follows. In Sec. II we present the variational mp-mh configuration mixing method together with its restriction to the case of pairing correlations. Results obtained for pairing-type correlations in ^{116}Sn, ^{106}Sn, and ^{100}Sn are presented and discussed in Sec. III. Summary and conclusions are given in Sec. IV.

II. GENERAL FORMALISM

In this part, we present the derivation of the variational mp-mh configuration mixing method applied to the ground state description of even-even nuclei. We have considered pertinent to detail it here first, as this approach is not commonly used in nuclear physics, contrary to atomic and molecular physics. Moreover, some features of the method are specific to nuclear physics, such as the existence of two kinds of particles and the occurrence of rearrangement terms coming from the density dependence of the phenomenological effective nucleon-nucleon interaction.

The variational mp-mh configuration mixing method is a self-consistent approach that generalizes the usual density-dependent Hartree-Fock (DDHF) approach [6,25] in order to take into account various types of nuclear correlations beyond the mean field in a unified way.

The trial wave function $|\Psi\rangle$ that describes nuclear states is taken as a linear combination

$$|\Psi\rangle = \sum_{\alpha_\pi \alpha_\nu} A_{\alpha_\pi \alpha_\nu} \left|\phi_{\alpha_\pi} \phi_{\alpha_\nu}\right\rangle \tag{1}$$

of direct products

$$\left|\phi_{\alpha_\pi} \phi_{\alpha_\nu}\right\rangle \equiv \left|\phi_{\alpha_\pi}\right\rangle \otimes \left|\phi_{\alpha_\nu}\right\rangle \tag{2}$$

of proton and neutron Slater determinants $|\phi_{\alpha_\pi}\rangle$ and $|\phi_{\alpha_\nu}\rangle$. The indices π and ν stand for proton and neutron, respectively. Each Slater determinant $|\phi_{\alpha_\tau}\rangle$, $\tau = \pi, \nu$, is a multiple particle-hole (p-h) excitation $\alpha_\tau = (p_1 h_1, p_2 h_2, \ldots)_\tau$ of a HF-type reference state $|\phi_\tau\rangle$ built with orbitals $a^+_{\tau j}$:

$$\left|\phi_{\alpha_\tau}\right\rangle = \prod_i^{M_{\alpha_\tau}} \left(a^+_{\tau p_i} a_{\tau h_i}\right) |\phi_\tau\rangle, \qquad |\phi_\tau\rangle = \prod_h a^+_{\tau h} |0\rangle, \tag{3}$$

where the index $h(p)$ denotes occupied (unoccupied) orbitals in $|\phi_\tau\rangle$.

In Eq. (1), the $A_{\alpha_\pi\alpha_\nu}$ are mixing coefficients. One notices that they are not taken as products of a proton and a neutron coefficient. The splitting of the mixing coefficients into the product of a proton and a neutron coefficient only occurs when the proton-neutron residual interaction is neglected. Therefore, in the most general case, $|\Psi\rangle$ is not the direct product of a proton and of a neutron wave function. It assumes the most general form compatible with the separate conservation of proton and neutron numbers. In Eq. (3), $M_{\alpha_{\pi(\nu)}}$ indicates what we will call the excitation order of the Slater $|\phi_{\alpha_\tau}\rangle$, that is, the number of p-h excitations applied to $|\phi_\tau\rangle$. The summation in Eq. (1) includes the HF-type reference state which is obtained for $M_{\alpha_\pi} = M_{\alpha_\nu} = 0$. The p-h excitations are restricted to those combinations conserving the quantum numbers associated with the symmetries imposed on the nuclear wave function. In the present work, they have been taken as the parity symmetry and the axial symmetry around the Oz axis. Also, a finite number of unoccupied p states are taken into account. Therefore, the number of configurations included in Eq. (1) is finite.

The state (1) depends on two sets of unknown quantities which are taken as variational parameters: the mixing coefficients $A_{\alpha_\pi\alpha_\nu}$ and the single-particle states $a^+_{\tau j}$ entering the Slater determinants of Eq. (3). They are determined by applying a variational principle to the energy functional:

$$\begin{aligned}\mathcal{F}(\Psi) &= \langle\Psi|\hat{H}[\rho]|\Psi\rangle - \lambda\langle\Psi|\Psi\rangle \\ &= \sum_{\alpha_\pi\alpha_\nu} A^*_{\alpha_\pi\alpha_\nu} A_{\alpha'_\pi\alpha'_\nu}\langle\phi_{\alpha_\pi}\phi_{\alpha_\nu}|\hat{H}[\rho] - \lambda|\phi_{\alpha'_\pi}\phi_{\alpha'_\nu}\rangle. \end{aligned} \quad (4)$$

The operator $\hat{H}[\rho]$ is the many-body Hamiltonian built with the two-body effective interaction $\hat{v}_{12}$:

$$\begin{aligned}\hat{H}[\rho] &= \sum_{ij}\langle i|\frac{\hat{p}^2}{2M}|j\rangle a^+_i a_j + \frac{1}{4}\sum_{ijkl}\langle ij|\hat{v}[\rho]|\tilde{kl}\rangle a^+_i a^+_j a_l a_k \\ &\equiv \hat{K} + \hat{V}[\rho] \end{aligned} \quad (5)$$

and the term proportional to λ is introduced in order to fix the normalization of $|\Psi\rangle$. The interaction $\hat{v}_{ij}$ is supposed to depend on the neutron+proton nuclear density distribution $\rho(\vec{r})$. Hence the notations $\hat{v}[\rho]$ and $\hat{H}[\rho]$. As mentioned in the Introduction, the density $\rho(\vec{r})$ used in the two-body interaction will be taken as the one-body density $\rho(\vec{r})$ associated with the correlated wave function $|\Psi\rangle$:

$$\rho(\vec{r}) = \langle\Psi|\hat{\rho}(\vec{r})|\Psi\rangle, \quad (6)$$

with $\hat{\rho}(\vec{r}) = \sum_{i=1}^{A}\delta(\vec{r} - \vec{r}_i)$. This prescription is arbitrary since there is no justification for employing the density of the correlated state $|\Psi\rangle$ within an energy density functional which is originally defined in the context of the mean-field theory. However, as pointed out in the Introduction, this choice has the advantage of introducing in a natural way the rearrangement terms that are essential for obtaining realistic matrix elements for the mean field and for the residual interaction [6,21–24]. Let us mention that the present prescription is consistent with the one adopted in the application of the VAP procedure of Refs. [9–11].

By performing independent variations of the mixing coefficients $A_{\alpha_\pi\alpha_\nu}$ and of the single-particle wave functions $\varphi_{\tau j}$ associated with the operators $a^+_{\tau j}$, one gets the two extrema conditions:

$$\begin{cases} \left.\dfrac{\partial\mathcal{F}(\Psi)}{\partial A^*_{\alpha_\pi\alpha_\nu}}\right|_{\varphi_{\tau j}\ \text{fixed}} = 0, \\ \left.\dfrac{\partial\mathcal{F}(\Psi)}{\partial\varphi^*_{\tau j}}\right|_{A_{\alpha_\pi\alpha_\nu}\ \text{fixed}} = 0. \end{cases} \quad (7)$$

Following the derivation in Appendix A, the first condition in Eq. (7) leads to the secular equation:

$$\sum_{\alpha'_\pi\alpha'_\nu}\mathcal{H}_{\alpha_\pi\alpha_\nu,\alpha'_\pi\alpha'_\nu}A_{\alpha'_\pi\alpha'_\nu} = \lambda A_{\alpha_\pi\alpha_\nu}, \quad (8)$$

where the Hamiltonian matrix $\mathcal{H}$ is defined by

$$\mathcal{H}_{\alpha_\pi\alpha_\nu,\alpha'_\pi\alpha'_\nu} = \langle\phi_{\alpha_\pi}\phi_{\alpha_\nu}|\hat{H} + \sum_{mn\tau}\Re^\tau_{mn}a^+_{\tau m}a_{\tau n}|\phi_{\alpha'_\pi}\phi_{\alpha'_\nu}\rangle, \quad (9)$$

with

$$\Re^\tau_{mn} = \int d^3\vec{r}\,\varphi^*_{\tau m}(\vec{r})\varphi_{\tau n}(\vec{r})\langle\Psi|\frac{\partial\hat{V}}{\partial\rho(\vec{r})}|\Psi\rangle, \quad (10)$$

and

$$\frac{\partial\hat{V}[\rho]}{\partial\rho(\vec{r})} = \frac{1}{4}\sum_{ijkl}\langle ij|\frac{\partial V[\rho]}{\partial\rho(\vec{r})}|\tilde{kl}\rangle a^+_i a^+_j a_l a_k. \quad (11)$$

As Eq. (10) shows, the quantities $\Re^\tau_{mn}$ are the matrix elements of a one-body Hamiltonian. One now expresses the Hamiltonian $\hat{H}[\rho]$ as the sum of the proton, neutron, and proton-neutron contributions:

$$\hat{H}[\rho] = \hat{H}^\pi[\rho] + \hat{H}^\nu[\rho] + \hat{V}^{\pi\nu}[\rho]. \quad (12)$$

Then, Eq. (9) takes the form

$$\begin{aligned}&\sum_{\alpha_\pi} A_{\alpha_\pi\alpha'_\nu}\Big(\langle\phi_{\alpha'_\pi}|\hat{H}^\pi[\rho]|\phi_{\alpha_\pi}\rangle \\ &\quad + \sum_{mn}\Re^\pi_{mn}(\rho,\sigma)\langle\phi_{\alpha'_\pi}|a^+_m a_n|\phi_{\alpha_\pi}\rangle\Big) \\ &\quad + \sum_{\alpha_\nu} A_{\alpha'_\pi\alpha_\nu}\Big(\langle\phi_{\alpha'_\nu}|\hat{H}^\nu[\rho]|\phi_{\alpha_\nu}\rangle \\ &\quad + \sum_{mn}\Re^\nu_{mn}(\rho,\sigma)\langle\phi_{\alpha'_\nu}|a^+_m a_n|\phi_{\alpha_\nu}\rangle\Big) \\ &\quad + \sum_{\alpha_\pi\alpha_\nu} A_{\alpha_\pi\alpha_\nu}\langle\phi_{\alpha'_\pi}\phi_{\alpha'_\nu}|\hat{V}^{\pi\nu}[\rho]|\phi_{\alpha_\pi}\phi_{\alpha_\nu}\rangle = \lambda A_{\alpha'_\pi\alpha'_\nu}. \end{aligned} \quad (13)$$

In Eq. (13), σ denotes the two-body correlation function defined by Eq. (19) below.

From Eq. (13), one sees that the Hamiltonian matrix $\mathcal{H}$ contains three different contributions:

(i) A proton contribution involving configurations $|\phi_{\alpha_\pi}\phi_{\alpha_\nu}\rangle$ and $|\phi_{\alpha'_\pi}\phi_{\alpha'_\nu}\rangle$ with the same neutron content: $|\phi_{\alpha_\nu}\rangle = |\phi_{\alpha'_\nu}\rangle$

(ii) A neutron contribution involving configurations $|\phi_{\alpha_\pi}\phi_{\alpha_\nu}\rangle$ and $|\phi_{\alpha'_\pi}\phi_{\alpha'_\nu}\rangle$ with the same proton content: $|\phi_{\alpha_\pi}\rangle = |\phi_{\alpha'_\pi}\rangle$
(iii) A proton-neutron contribution.

The first two contributions include rearrangement terms $\Re^\tau_{mn}$ coming from the density-dependence of the effective force used. Because of these terms and of the dependence of $\hat{H}^\tau[\rho]$ on the density ρ, the secular equation (8) is a highly nonlinear equation that does not reduce to the simple diagonalization of the Hamiltonian matrix $\mathcal{H}$. We give later on more details about the way this equation can be solved.

From Eq. (13), one sees that in the variational mp-mh configuration mixing method, the residual interaction has two components. The first one originates from the matrix elements $\langle\phi_{\alpha'_\tau}|\hat{H}^\tau[\rho]|\phi_{\alpha_\tau}\rangle$ between configurations $|\phi_{\alpha_\tau}\rangle$ and $|\phi_{\alpha'_\tau}\rangle$ differing by 2p-2h excitations and from the matrix elements $\langle\phi_{\alpha'_\pi}\phi_{\alpha'_\nu}|\hat{V}^{\pi\nu}[\rho]|\phi_{\alpha_\pi}\phi_{\alpha_\nu}\rangle$. The second one is composed of rearrangement terms between two configurations differing by 1p-1h excitations.

Equation (8) will be used to calculate the mixing coefficients $A_{\alpha_\pi\alpha_\nu}$ for known orbitals $a^+_{\tau j}$ and the total energy associated with the correlated state. The second condition of Eq. (7) will serve to determine the representation used in the Slater determinants of Eq. (3). This condition applies because only a finite set of single-particle orbitals and a truncated excitation order are used and, therefore, the correlated wave function $|\Psi\rangle$ spans only a restricted part of the full many-body Hilbert space. Expanding the $a^+_{\tau j}$ over a given fixed single-particle basis denoted by c^+_n

$$a^+_{\tau j} = \sum_n C_{n,\tau j} c^+_n, \tag{14}$$

the variation with respect to $\{\varphi_{\tau j}\}$ is equivalent to the variation of the coefficients $C_{n,\tau j}$. Hence, the second equation (7) is equivalent to

$$\frac{\partial \mathcal{F}(\Psi)}{\partial C^*_{n,\tau j}} = 0. \tag{15}$$

As shown in Appendix B, this leads to the condition

$$\langle\Psi|\left[\hat{H} + \int \langle\Psi|\frac{\partial \hat{V}[\rho]}{\partial\rho(\vec{r})}|\Psi\rangle\hat{\rho}(\vec{r})d^3\vec{r}, a^+_k a_l\right]|\Psi\rangle = 0, \tag{16}$$

where

$$\langle\Psi|\frac{\partial \hat{V}[\rho]}{\partial\rho(\vec{r})}|\Psi\rangle = \frac{1}{4}\sum_{mnpr}\langle mn|\frac{\partial \hat{V}[\rho]}{\partial\rho(\vec{r})}|\widetilde{pr}\rangle\langle\Psi|a^+_m a^+_n a_r a_p|\Psi\rangle. \tag{17}$$

Using the following definitions for the one-body density matrix ρ associated with the correlated state $|\Psi\rangle$

$$\rho_{ij} = \langle\Psi|a^+_j a_i|\Psi\rangle \tag{18}$$

and the two-body correlation matrix σ

$$\sigma_{ij,kl} = \langle\Psi|a^+_i a^+_k a_l a_j|\Psi\rangle - \rho_{ji}\rho_{lk} + \rho_{jk}\rho_{li}, \tag{19}$$

one can show that Eq. (16) is equivalent to the inhomogeneous HF-type equation

$$[h[\rho,\sigma],\rho] = G(\sigma). \tag{20}$$

Here, $h[\rho,\sigma]$ is the one-body mean-field Hamiltonian built with the one-body density ρ and the two-body correlation function σ:

$$h_{ij}[\rho,\sigma] = \langle i|K|j\rangle + \Gamma_{ij}[\rho] + \partial\Gamma_{ij}[\rho] + \partial\Gamma_{ij}[\sigma], \tag{21}$$

with

$$\Gamma_{ij}[\rho] = \sum_{mn}\langle im|V[\rho]|\widetilde{jn}\rangle\rho_{nm}, \tag{22}$$

$$\partial\Gamma_{ij}[\rho] = \frac{1}{2}\sum_{mnpq}\langle mn|\frac{V[\rho]}{\partial\rho_{ji}}|\widetilde{pq}\rangle\rho_{pm}\rho_{qn}, \tag{23}$$

$$\partial\Gamma_{ij}[\sigma] = \frac{1}{2}\sum_{mnpq}\langle mn|\frac{V[\rho]}{\partial\rho_{ji}}|\widetilde{pq}\rangle\sigma_{mp,nq}, \tag{24}$$

and

$$\begin{aligned} G_{kl}(\sigma) = &\frac{1}{2}\sum_{imn}\langle im|V[\rho]|\widetilde{kn}\rangle\sigma_{il,mn} \\ &-\frac{1}{2}\sum_{imn}\langle ml|V[\rho]|\widetilde{ni}\rangle\sigma_{ki,mn}. \end{aligned} \tag{25}$$

From Eq. (25), one sees that G_{kl} is an anti-Hermitian matrix.

The fourth term on the right-hand side of Eq. (21) is unusual in the definition of the mean field. It is a rearrangement field that makes the nuclear mean field dependent on not only the one-body matrix ρ but also the correlation matrix σ. Equation (20) shows that the single-particle orbitals a^+_i depend on σ also through the matrix $G(\sigma)$. By introducing the "natural basis" associated with the mp-mh wave function $|\Psi\rangle$, i.e., the representation $|\mu\rangle$ that diagonalizes the one-body density matrix ρ

$$\rho_{\mu\nu} = \delta_{\mu\nu}n_\mu, \tag{26}$$

this equation can be cast into the form

$$\hat{h}[\rho,\sigma]|\varphi_\mu\rangle = \sum_\nu|\varphi_\nu\rangle\epsilon_{\nu\mu} + |X_\mu(\sigma)\rangle, \tag{27}$$

where $|X_\mu(\sigma)\rangle$ depend on the matrix $G(\sigma)$. This equation has the same structure as the partial differential equations solved in atomic and molecular physics. Equation (27) can be used to determine the natural states $|\mu\rangle$. Then, the single-particle states $|i\rangle$ can be derived, since they are related to the $|\mu\rangle$ by a unitary transformation depending only on the mixing coefficients A.

In the first application made in this work, we did not solve the full equation (27) because of the complicated structure of $G(\sigma)$. That is, we neglected the dependence of $h[\rho,\sigma]$ on σ and omitted the last term in Eq. (27). With this approximation, correlations influence the single-particle states $|i\rangle$ only through the one-body density matrix ρ. Since the simplified equation (27) is still nonlinear, the states $|\mu\rangle$ are obtained using an iterative procedure: One starts from a HF calculation that gives a first set of single-particle orbitals. With the correlated wave function $|\Psi\rangle$ solution of Eq. (8), one calculates the correlated one-body density $\rho_{ij} = \langle\Psi|a^+_j a_i|\Psi\rangle$ that is then

used to calculate h. The diagonalization of h gives a new set of single-particle orbitals. With this new set of orbitals, one solves again Eq. (8) and the procedure is applied until convergence. The convergence is obtained when the variation of all matrix elements of ρ between two iterations is less than a defined accuracy.

The existence of Eq. (20), even when approximated by the scheme outlined just above, is a very important feature of the mp-mh formalism. It expresses the fact that the single-particle states entering the definition of $|\Psi\rangle$ depend on the coupling between the HF-type ground state and mp-mh excited configurations. Therefore, the self-consistent single-particle orbitals incorporate a part of the residual interaction beyond the usual HF single-particle potential. This should have the consequence of minimizing the effects of the residual interaction and should allow one to truncate the expansion of $|\Psi\rangle$ to low p-h excitation order [16,17,26]. In this sense, the single-particle structure derived from Eq. (20) appears as the most adapted for describing both the mean field and the correlation content of $|\Psi\rangle$. Let us note at this stage that the strong short-range correlations due to the repulsive core of the nucleon-nucleon interaction are already absorbed in the phenomenological effective interaction. Therefore, only correlations associated with long-range correlations have to be included, explaining why the above-mentioned truncation in the expansion of the wave function can be made. These remarks are of course crucial in view of the tractability of the mp-mh configuration mixing method.

It must be emphasized that the mp-mh configuration mixing method does not make use of an inert core. This is an important feature of the method, because the matrix elements that couple the occupied deep single-particle states in $|\phi_\tau\rangle$ with high-lying unoccupied ones are not negligible. For instance, taking the Fourier transform of the central part of the Gogny force shows that occupied single-particle states can couple to unoccupied states up to 80 MeV excitation energy. In fact, these matrix elements are expected to contribute significantly to the renormalization of the single-particle states due to correlations.

Since the correlated wave function $|\Psi\rangle$ is derived from a variational principle applied to the total energy of the system, it will describe the state having the lowest energy for a given set of quantum numbers. Then, the mp-mh formalism formulated here can be applied to the description of ground states as well as of yrast nuclear states. These will be obtained as the solution with the lowest eigenvalue of λ in Eq. (8). Excited states $|\Psi_1\rangle$ having the same quantum numbers can be obtained by adding constraints $-\lambda_1\langle\Psi_0|\Psi\rangle$ to the functional $\mathcal{F}$ of Eq. (4), whose purpose is to impose $|\Psi\rangle$ to be orthogonal to the ground state $|\Psi_0\rangle$, and more generally, by adding a set of constraints $-\sum_{j=0}\lambda_j\langle\Psi_j|\Psi\rangle$, where $|\Psi_j\rangle$ are the ground state and excited states with lower energy than that of the excited state $|\Psi\rangle$ that is looked for. This kind of extension will not be further discussed in this paper. A reasonable approximation of low energy excited states $|\Psi_1\rangle$ should, however, be obtained by taking the second, third, etc. lower energy solutions of Eq. (8). One expects this approximation to be good if the single-particle structure associated with $|\Psi_1\rangle$ is not very different from the one associated with $|\Psi_0\rangle$.

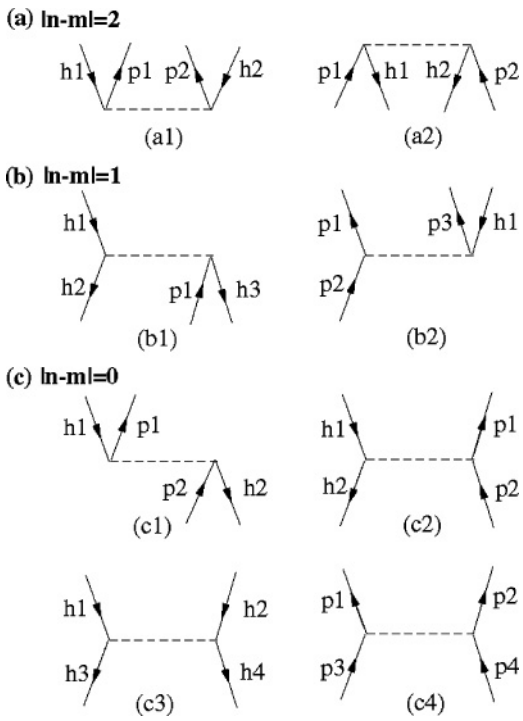

FIG. 1. Configuration mixing diagrams.

Two-body residual correlations are introduced in the mp-mh configuration mixing method from matrix elements $\langle\phi_{\alpha'_\pi}\phi_{\alpha'_\nu}|\hat{V}[\rho]|\phi_{\alpha_\pi}\phi_{\alpha_\nu}\rangle$ appearing in the right-hand side of Eq. (9) between configurations that differ from two particles in two different orbitals. These matrix elements can be represented by Feynman diagrams [27] as in Fig. 1, where the total order of excitation of the configuration $|\phi_{\alpha_\pi}\phi_{\alpha_\nu}\rangle(|\phi_{\alpha'_\pi}\phi_{\alpha'_\nu}\rangle)$ is denoted by n (m). In all diagrams, p (h) stands for particle (hole) states. The evaluation of the many-body matrix elements $\langle\phi_{\alpha'_\pi}\phi_{\alpha'_\nu}|\hat{V}[\rho]|\phi_{\alpha_\pi}\phi_{\alpha_\nu}\rangle$ in terms of the two-body matrix elements lead to three nontrivial cases for (a) $|n-m|=2$, (b) $|n-m|=1$, and (c) $|n-m|=0$. In the three cases, the two many-body configurations $|\phi_{\alpha_\pi}\phi_{\alpha_\nu}\rangle$ and $|\phi_{\alpha'_\pi}\phi_{\alpha'_\nu}\rangle$ have to differ exactly by 2p-2h excitation, otherwise the matrix element is zero.

Diagrams (a1) and (a2) are those that introduce correlations in the mp-mh configuration mixing wave function. In the description of ground states, they mix in particular the HF-type reference state with 2p-2h configurations. More generally, they couple mp-mh with (m+2)p-(m+2)h configurations. Diagrams (a1) and (a2) are those responsible for ground state correlations in the RPA theory, where they generate virtual 2p-2h excitations (see, for example, Ref. [1]). In the case where p_2 and h_2 are the time-reversed states of p_1 and h_1, respectively, these diagrams create Cooper pairs from the noncorrelated state.

Diagrams (b1) and (b2) are rarely introduced in microscopic approaches. They describe the influence of a p-h pair annihilation (creation) on the propagation of a hole (particle). They allow one to introduce the coupling between individual and collective motion, i.e., the so-called particle-vibration coupling.

Diagrams (c1)–(c4), which appear in the mp-mh configuration mixing approach between Slater determinants with the same order of excitation, are encountered in various approaches. On the one hand, diagrams (c1) and (c2) are characteristic of RPA-type correlations. They are introduced in ph-RPA through the well-known A submatrix of the RPA matrix (see, for example, Ref. [1]). Diagram (c1) represents the direct part and diagram (c2) the exchange part of the same two-body matrix element. Diagram (c1) describes the annihilation of a p-h pair and the creation of another one. In diagram (c2), a p-h pair is scattered from one state to another one. On the other hand, diagrams (c3) and (c4) appear in the pp(hh)-RPA and in QRPA. In such formalism, they describe pairing vibrations for collective states [1]. In the particular case where particles are in time-reversed states, they describe the pair diffusion mechanism of the BCS and HFB approaches.

Let us end this section by giving the definition of the correlation energy we will use. The correlation energy $E_{\rm corr}$ will be taken as the difference between the total energy $\mathcal{E}(\Psi) = \langle\Psi|\hat{H}|\Psi\rangle$ of the correlated system defined in Eq. (A20) of Appendix A and the energy of the simple HF method $\mathcal{E}_0^{\rm HF} = \langle\phi_0|\hat{H}|\phi_0\rangle$:

$$E_{\rm corr} = \mathcal{E}(\Psi) - \mathcal{E}_0^{\rm HF}, \tag{28}$$

where $|\phi_0\rangle$ is such that $\langle\delta\phi_0|\hat{H}|\phi_0\rangle = 0$.

III. PAIRING CORRELATION DESCRIPTION USING THE mp-mh FORMALISM

A. Residual pairing Hamiltonian

In this part, we apply the mp-mh configuration mixing formalism for the description of the usual proton-proton and neutron-neutron pairing correlations.

As already mentioned in the Introduction, the description in terms of mean field plus residual pairing Hamiltonian has played a very important role in the understanding of nuclear structure and low-energy spectroscopy. The commonly used BCS approximation or its HFB extension, which solves this problem in an approximate way, suffer from defects, as for example the nonconservation of particle number, which is in general invoked because of the inability of such an approach to describe weak pairing regimes.

In the exact solution of a pairing Hamiltonian formulated by Richardson [28], eigensolutions with seniority $s = 0$ and $s = 2$ compete energetically. Let us note that the seniority quantum number gives the number of unpaired nucleons or twice the number of broken pairs in even particle systems. In the language of BCS or HFB approximations, this means that the exact treatment produces four-quasiparticle excitations lying lower in energy than two-quasiparticle excitations. This behavior is never observed in BCS or HFB approaches, where four-quasiparticle excitations are always far too high in energy (the first two-quasiparticle excitation corresponding to pair breaking). Therefore, it looks interesting to exhibit the relationship and differences between the PBCS solution, the mp-mh configuration mixing solution and the exact solution of the pairing Hamiltonian.

In a standard way, when no proton-neutron pairing correlation is included, the total BCS wave function is expressed as the direct product of a proton by a neutron BCS wave function:

$$|\mathrm{BCS}\rangle = |\mathrm{BCS}\rangle_\pi \times |\mathrm{BCS}\rangle_\nu. \tag{29}$$

In second quantization, for even-even nuclei, each BCS wave function $|\mathrm{BCS}\rangle_\tau$ ($\tau \equiv \pi$ or ν) is written as

$$|\mathrm{BCS}\rangle_\tau = \mathcal{N}_\tau e^{B_\tau^+}|0\rangle_\tau, \tag{30}$$

where $|0\rangle_\tau$ represents the proton or neutron vacuum.

In Eq. (30), $\mathcal{N}_\tau$ is the normalization constant, and B_τ^+ is a collective pair creation operator:

$$\mathcal{N}_\tau = \prod_{j>0}\cos\theta_{\tau j}, \quad B_\tau^+ = \sum_{j>0} tg\theta_{\tau j} b_{\tau j}^+, \tag{31}$$

with $\cos\theta_{\tau j} \equiv u_{\tau j}$ and $\sin\theta_{\tau j} \equiv v_{\tau j}$ ($u_{\tau j}$ and $v_{\tau j}$ being the usual variational parameters of the BCS approach). The $b_{\tau j}^+$ operator represents the pair creation operator

$$b_{\tau j}^+ = a_{\tau j}^+ a_{\tau\bar{j}}^+, \tag{32}$$

where the $\{a_{\tau j}, a_{\tau j}^+\}$ are defined in Eq. (14). In this work, a pair of nucleons is defined as two nucleons in time-reversed states, and it is coupled to a total angular momentum projection and parity $K^p = 0^+$. Expanding the exponential of Eq. (30), $|\mathrm{BCS}\rangle_\tau$ can be written as

$$|\mathrm{BCS}\rangle_\tau = \sum_{N=0}^{\infty}\frac{(B_\tau^+)^N}{N!}|0\rangle. \tag{33}$$

The $|\mathrm{BCS}\rangle_\tau$ wave function decomposes into wave functions with different numbers of particles $2N$. It is always possible to extract from Eq. (33) the part of $|\mathrm{BCS}\rangle_\tau$ having the good particle number $2N$, that is,

$$|\phi_{2N}\rangle_\tau = \mathcal{N}_\tau \sum_{0<j_1<j_2<\cdots<j_N} tg\theta_{\tau j_1}\ldots tg\theta_{\tau j_N} b_{\tau j_1}^+\ldots b_{\tau j_N}^+|0\rangle. \tag{34}$$

Defining the HF-type state with $2N$ particles as

$$|\mathrm{HF}\rangle_\tau = \prod_{h=1}^{N} b_{\tau h}^+|0\rangle, \tag{35}$$

one finds

$$|\phi_{2N}\rangle_\tau = \mathcal{N}'_\tau \sum_{n=0}^{\infty}\sum_{\substack{0<p_1<\cdots<p_n\\0<h_1<\cdots<h_n}}\frac{tg\theta_{\tau p_1}\ldots tg\theta_{\tau p_n}}{tg\theta_{\tau h_1}\ldots tg\theta_{\tau h_n}} \times\prod_{k=1}^{n}\left(b_{\tau p_k}^+ b_{\tau h_k}\right)|\mathrm{HF}\rangle, \tag{36}$$

where $\mathcal{N}'_\tau = \mathcal{N}_\tau\prod_h tg\theta_{\tau h} = \prod_{h>0}\sin\theta_{\tau h}\prod_{p>0}\cos\theta_{\tau p}$. The wave function $|\phi_{2N}\rangle$ clearly is the projection of $|\mathrm{BCS}\rangle$ onto the good particle number $2N$. One sees that such a wave function is a superposition of configurations corresponding to excitations of nucleon pairs. Equation (36) shows that the projected BCS wave function is a subset of the general mp-mh wave function of Eq. (1), containing only certain types of configurations and with particular mixing coefficients that are products of particle

and hole coefficients. Because of the particular form of mixing coefficients, $|\phi_{2N}\rangle_\tau$ is also less general than the exact solution of pairing Hamiltonian formulated by Richardson.

In the framework of the variational mp-mh configuration mixing method, one considers as a trial wave function the reduction of Eq. (1) built only with the excited pair configurations that are relevant for the description of pairing correlations with particle number conservation. Such kind of trial wave function mimics the exact solution of pairing Hamiltonian. Then, proton and neutron Slater determinants are written as

$$|\phi_{\alpha_\tau}\rangle = \prod_{i=1}^{M_{\alpha_\tau}} \left(b^+_{\tau p_i} b_{\tau h_i}\right)|\phi_\tau\rangle. \tag{37}$$

Here, M_{α_τ} designates the number of excited pairs in the configuration $|\phi_{\alpha_\tau}\rangle$. As shown in Appendix C, without residual proton-neutron interaction, the mixing coefficients $A_{\alpha_\pi\alpha_\nu}$ split into the direct product of a proton coefficient and a neutron one. Then, the correlated wave function takes the particular form

$$|\Psi'\rangle = \left|\Psi^k_\pi\right\rangle \otimes \left|\Psi^j_\nu\right\rangle, \tag{38}$$

where $|\Psi^i_\tau\rangle = \sum_{\alpha_\tau} U^\tau_{\alpha_\tau,i}|\phi_{\alpha_\tau}\rangle$ and $\sum_{\alpha_\tau}|U^\tau_{\alpha_\tau,i}|^2 = 1$. For the description of ground states of even-even nuclei, the proton and neutron correlated wave functions $|\Psi^p_\pi\rangle$ and $|\Psi^n_\nu\rangle$ are coupled to $K^p = 0^+$:

$$|\Psi'\rangle_{0^+} = \left|\Psi^p_\pi\right\rangle_{0^+} \otimes \left|\Psi^n_\nu\right\rangle_{0^+}. \tag{39}$$

One defines the functional $\mathcal{F}(\Psi')$ as

$$\mathcal{F}(\Psi') = \langle\Psi'|\hat{H}[\rho]|\Psi'\rangle - \lambda_\pi\left\langle\Psi^p_\pi\middle|\Psi^p_\pi\right\rangle - \lambda_\nu\left\langle\Psi^n_\nu\middle|\Psi^n_\nu\right\rangle. \tag{40}$$

The first equation of Eq. (7) is equivalent to

$$\frac{\partial\mathcal{F}(\Psi')}{\partial U^{p*}_{\alpha'_\pi}} = 0, \qquad \frac{\partial\mathcal{F}(\Psi')}{\partial U^{n*}_{\alpha'_\nu}} = 0. \tag{41}$$

One expresses the Hamiltonian $\hat{H}[\rho]$ as the sum of proton, neutron, and proton-neutron contributions:

$$\hat{H}[\rho] = \hat{H}^\pi[\rho] + \hat{H}^\nu[\rho] + \hat{V}^{\pi\nu}[\rho]. \tag{42}$$

The density-dependent term of the D1S Gogny force acts only between proton and neutron configurations. The associated rearrangement term is noted as $\delta\hat{H}_{\pi\nu}[\rho]$.

Following the same method as for the general formalism, the variational principle yields the coupled set of equations

$$\sum_{\alpha'_\pi} U^p_{\alpha'_\pi}\left[\left\langle\phi_{\alpha_\pi}\middle|\hat{H}^\pi\middle|\phi_{\alpha'_\pi}\right\rangle + \mathcal{E}^{\pi\nu}_{\alpha'_\pi}\delta_{\alpha_\pi\alpha'_\pi}\right] = (\lambda_\pi - \mathcal{E}_\nu)U^p_{\alpha_\pi}, \tag{43}$$

$$\sum_{\alpha'_\nu} U^n_{\alpha'_\nu}\left[\left\langle\phi_{\alpha_\nu}\middle|\hat{H}^\nu\middle|\phi_{\alpha'_\nu}\right\rangle + \mathcal{E}^{\pi\nu}_{\alpha'_\nu}\delta_{\alpha_\nu\alpha'_\nu}\right] = (\lambda_\nu - \mathcal{E}_\pi)U^n_{\alpha_\nu}. \tag{44}$$

Equation (43) determines proton mixing coefficients, and Eq. (44) neutron ones. The quantities $\mathcal{E}_\nu$ and $\mathcal{E}^{\pi\nu}_{\alpha_\pi}$ that appear in Eq. (43) are defined as

$$\mathcal{E}_\nu = \sum_{\alpha_\nu\alpha'_\nu} U^{n*}_{\alpha_\nu}U^n_{\alpha'_\nu}\left\langle\phi_{\alpha_\nu}\middle|\hat{H}^\nu\middle|\phi_{\alpha'_\nu}\right\rangle, \tag{45}$$

$$\mathcal{E}^{\pi\nu}_{\alpha_\pi} = \sum_{\alpha_\nu}\left(U^n_{\alpha_\nu}\right)^2\left\langle\phi_{\alpha_\pi}\phi_{\alpha_\nu}\middle|\hat{V}^{\pi\nu}[\rho] + \delta\hat{H}_{\pi\nu}[\rho]\middle|\phi_{\alpha_\pi}\phi_{\alpha_\nu}\right\rangle. \tag{46}$$

Similar expressions for $\mathcal{E}_\pi$ and $\mathcal{E}^{\pi\nu}_{\alpha_\nu}$ in Eq. (44) are obtained by exchanging π and ν indices in Eqs. (45) and (46), respectively.

Even though no proton-neutron residual interaction is taken into account, the two sets of Eqs. (45) and (46) are not fully decoupled because of the four terms $\mathcal{E}_\nu$, $\mathcal{E}_\pi$, $\mathcal{E}^{\pi\nu}_{\alpha'_\pi}$, and $\mathcal{E}^{\pi\nu}_{\alpha'_\nu}$. This means that the neutron solution depends on the proton solution and conversely.

B. Results without self-consistency

In this part, we discuss effects of pairing correlations concerning the description of ^{116}Sn, ^{106}Sn, and ^{100}Sn ground states using the variational mp-mh configuration mixing approach. The same interaction is used in the mean field and the residual part of the Hamiltonian, namely, the D1S Gogny force [29]. The correlated wave function contains only configurations corresponding to pair excitations. No proton-neutron residual interaction is taken into account. The residual part of the Hamiltonian is defined using the Wick decomposition of the many-body Hamiltonian $\hat{H}$ with respect to the uncorrelated state $|\phi_\pi\phi_\nu\rangle$.

In this section, we focus on the effect of the mp-mh configuration mixing. Results presented in this part have been obtained by solving only the first equation of Eq. (7), which determines mixing coefficients. We have performed one HF calculation followed by one diagonalization in the multiconfiguration space.

We have been interested in the convergence properties in multiconfiguration space, correlation energies [Eq. (28)], and the structure of correlated wave functions [Eq. (38)]. From a technical point of view, an 11-shell harmonic oscillator basis is used to expand single-particle states [see Eq. (14)], and axial symmetry is imposed. We will call level the twice-degenerated axially symmetric state containing two time-reversed nucleon states. Because calculations are performed in even-even nuclei for which $K^p = J^p = 0^+$ (with K the projection of the spin J onto the symmetry axis), the mp-mh nuclear states are even under the time-reversal symmetry $\hat{T}$. Furthermore, we restrict the multiconfiguration space by imposing the self-consistent symmetry $\hat{T}\hat{\Pi}_2$, where $\hat{\Pi}_2$ is the reflection with respect to the xOz plane. Using this symmetry, all matrix elements and mixing coefficients can be chosen real. Let us add that the two-body center of mass correction term has not been included in the effective interaction.

1. *Convergence properties in the multiconfiguration space*

Convergence properties, according to two criteria, have been studied for the description of ^{116}Sn, ^{106}Sn, and ^{100}Sn ground states: (i) the number of single-particle states included for the configuration mixing, assuming no core (all single-particle states under the Fermi level have always been taken into account) and (ii) the truncation in the expansion of the correlated wave function according to the total excitation order $M = M_{\alpha_\pi} + M_{\alpha_\nu}$, where M_{α_τ} defines the number of excited pairs for each isospin [see Eq. (37)].

Table I shows, for protons and neutrons, the number of Slater determinants restricted to $M_{\alpha_\tau} = 1$ or 2 and the total size

TABLE I. Number of proton π and neutron ν Slater determinants corresponding to one excited and two excited pairs and total dimensions following the criteria $M = M_{\alpha_\pi} + M_{\alpha_\nu} \leqslant 2$, for ^{100}Sn, ^{106}Sn, and ^{116}Sn. 286 proton and 286 neutron single-particle levels have been considered.

Nucleus	$(1\text{pair})_\pi$	$(1\text{pair})_\nu$	$(2\text{pairs})_\pi$	$(2\text{pairs})_\nu$	Dimension
^{100}Sn	6525	6525	10 179000	10 179000	62 946676
^{106}Sn	6525	7224	10 179000	12 531834	69 861184
^{116}Sn	6525	8349	10 179000	16 831584	81 502684

of the multiconfiguration space associated to $M \leqslant 2$. Proton and neutron valence spaces include the entire number of single-particle levels generated by an 11-shell harmonic oscillator basis, that is, 286 proton and 286 neutron doubly degenerate single-particle levels.

Columns 2–4 give the number of proton and neutron configurations corresponding to one and two excited pairs. In column 5, the indicated dimension includes configurations as $(0\text{pair})_\pi \otimes (0\text{pair})_\nu$, $(0\text{pair})_\pi \otimes (1\text{pair})_\nu$, $(1\text{pair})_\pi \otimes (0\text{pair})_\nu$, $(0\text{pair})_\pi \otimes (2\text{pairs})_\nu$, $(1\text{pair})_\pi \otimes (1\text{pair})_\nu$, $(2\text{pairs})_\pi \otimes (0\text{pair})_\nu$. Dimensions associated with three excited pair configurations are omitted because their effect is found negligible in our calculations for the three Sn isotopes.

The diagonalization of the Hamiltonian matrices of $\mathcal{H}$-type [see Eq. (9)] is accomplished using a very efficient technique developed for large-scale shell-model calculations [14,30]. This state-of-the-art method and the capabilities of present-day computers allow us to diagonalize matrices of the size presented in Table I in a reasonably fast way, which is a crucial point concerning the feasibility of the present variational mp-mh configuration mixing method.

The quantity for which it is obviously natural to be interested in is the convergence of the correlation energy [Eq. (28)]. Results are shown in Figs. 2 and 3 for ^{116}Sn, a nucleus containing large pairing correlations.

Figure 2 displays the evolution of the correlation energy, in absolute value and expressed in MeV, as a function of the number of proton single-particle levels (proton orbitals are ordered by increasing energy), for a fixed number of neutron configurations. All neutron configurations corresponding to 286 single-particle levels have been included. Full circles show the correlation energy for configurations containing only one excited pair: $(0\text{pair})_\pi \otimes (0\text{pair})_\nu$ and $(0\text{pair})_\pi \otimes (1\text{pair})_\nu$. Triangles indicate the result obtained with in addition two excited pairs: $(0\text{pair})_\pi \otimes (2\text{pairs})_\nu$, $(1\text{pair})_\pi \otimes (1\text{pair})_\nu$, and $(2\text{pairs})_\pi \otimes (0\text{pair})_\nu$. On each curve, the first point on the left is calculated for 25 proton levels for which only the 0 excited pair configuration occurs. This point gives an estimate of the neutron contribution to the total correlation energy, since in this case only neutrons are excited: $(0\text{pair})_\pi \otimes (0\text{pair})_\nu$, $(0\text{pair})_\pi \otimes (1\text{pair})_\nu$, and $(0\text{pair})_\pi \otimes (2\text{pairs})_\nu$. For this first point, neutron correlations coming from one excited pair configurations is $\simeq$2.5 MeV. Neutron two excited pair configurations bring an additional energy of $\simeq$1 MeV. As more and more proton single-particle levels are included, one observes that the correlation energy saturates. Analyzing the correlated wave function shows that most of the proton correlation energy comes from the proton single-particle states close to the Fermi level. For each curve, one sees that a change in the slope occurs for a number of proton single-particle levels near 50. One obtains that the eigensolution (black triangles) including additional two excited proton pair configurations and mixed two excited pair configurations brings an energy gain of about $\sim$1 MeV with respect to the eigensolution containing only one excited pair configurations. The contributions of three and more excited pair configurations are not shown on the figure because they are small. For instance, three excited pair configurations contribute less than 100 keV to the correlation energy.

Similarly, Fig. 3 shows the evolution of the correlation energy as a function of the number of neutron single-particle levels for a fixed number of proton configurations corresponding

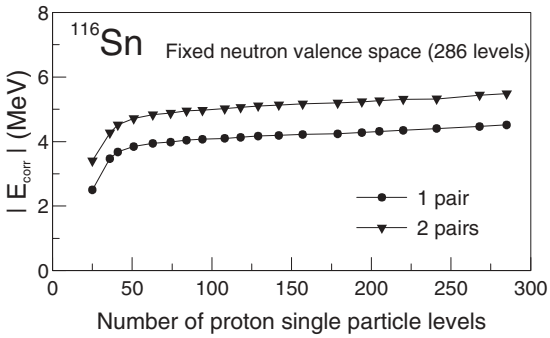

FIG. 2. Evolution of the correlation energy calculated with the mp-mh configuration mixing method, as a function of the proton valence space for ^{116}Sn.

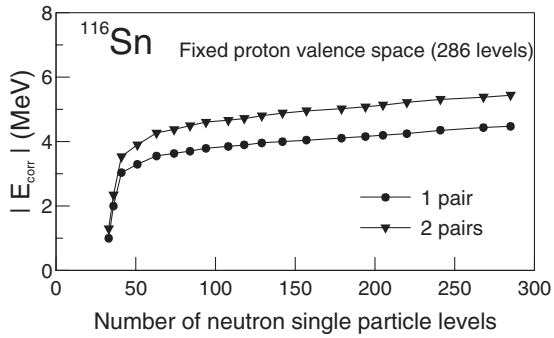

FIG. 3. Evolution of the correlation energy calculated with the mp-mh configuration mixing method, as a function of the neutron valence space for ^{116}Sn.

to 286 proton single-particle levels. As previously discussed, results are shown for wave functions including configurations up to one excited and two excited pairs. The left-most point on each curve, corresponding to 33 neutron single-particle levels, now gives an estimate of the contribution from the proton to the total correlation energy. Adding proton two excited pair configurations is less crucial than in the case of neutron ones as the correlation energy gain is only $\simeq$ 200 keV. Again, one observes a change in the slope around 50 neutron single-particle levels. The slope change is much sharper than in Fig. 2, which indicates that neutron correlations are stronger than proton ones. One sees that the convergence of the correlation energy as a function of the number of neutron levels is less good than in Fig. 2. This slow convergence of the correlation energy can be understood from the magnitude of the ranges (0.7 and 1.2 fm) of the Gaussian part of the Gogny force. When pairing correlations are strong, pairs involve single-particle levels up to $\simeq$100 MeV excitation energy. Let us note that a similar behavior is observed in HFB calculations.

Similar calculations have been done for ^{106}Sn and ^{100}Sn. As expected, the behavior of the correlation energy as a function of the proton valence space is similar to the one of ^{116}Sn. In contrast, the convergence of the correlation energy with the size of the neutron valence space is somewhat different for ^{106}Sn and ^{100}Sn. For ^{100}Sn, convergence properties according to the size of neutron valence space resemble the ones associated to proton valence space (see Fig. 2), since ^{100}Sn is a doubly magic $N = Z$ nucleus. The solution containing two excited pair configurations brings an energy gain of about $\simeq$300 keV on top of the one excited pair configurations. This clearly indicates that two excited pair configurations are less important for the description of the ^{100}Sn ground state than in ^{116}Sn. ^{106}Sn appears as an intermediate case between ^{116}Sn and ^{100}Sn, where the magnitude of neutron correlations is stronger than in ^{100}Sn and smaller than in ^{116}Sn. The slope changes observed on the left of curves such as those in Figs. 2 and 3 are smaller than in ^{116}Sn. Adding the contribution of the two excited pair configurations brings an additional energy of around 700 keV instead of the 1 MeV observed in ^{116}Sn and 300 keV in ^{100}Sn.

The main conclusions of this study can be summarized as follows: (i) Most correlations come from excited configurations implying single-particle states close to the Fermi level and are provided by configurations built with one excited pair. (ii) Two excited pair configurations are essential in ^{116}Sn and ^{106}Sn ground states. (iii) Three excited pair configurations can be neglected.

2. *Correlation energy*

We discuss here the magnitude and origin of the correlation energy obtained in the three Sn isotopes. Unless otherwise mentioned, all available proton and neutron single-particle states are taken into account (286 doubly degenerated levels for each kind of nucleon) and the multiconfiguration space includes configurations up to two excited pairs.

The second column of Table II displays the absolute value of the total correlation energy $|E_{\rm corr}|$ for ^{116}Sn, ^{106}Sn, and ^{100}Sn. One sees that ^{116}Sn is the most correlated nucleus and ^{100}Sn the less one: $|E_{\rm corr}| = 5.44$ MeV against $|E_{\rm corr}| = 3.67$ MeV, respectively. The third column gives the associated neutron contribution noted $|E_{\rm corr}^{\rm neutron}|$. The neutron contribution is extracted from a calculation in which neutrons are excited whereas protons are in the HF configuration. When one goes from ^{100}Sn to ^{116}Sn, the neutron correlation energy increases. Let us note that the usual BCS or HFB approximations are unable to find correlations in ^{100}Sn and more generally when the pairing strength is small compared to the value of the gap between the last occupied level and the first unoccupied level in the HF approach.

TABLE II. Absolute values of total correlation energy $|E_{\rm corr}^{\rm total}|$ and neutron contribution $|E_{\rm corr}^{\rm neutron}|$ for ^{100}Sn, ^{106}Sn, and ^{116}Sn. Energies are expressed in MeV.

Nucleus	$\lvert E_{\rm corr}^{\rm total}\rvert$	$\lvert E_{\rm corr}^{\rm neutron}\rvert$
^{100}Sn	3.67	1.90
^{106}Sn	4.62	2.88
^{116}Sn	5.44	3.74

The difference between $E_{\rm corr}$ and $E_{\rm corr}^{\rm neutron}$ is of the same order of magnitude for the three Sn isotopes, about 1.7 MeV. This indicates that correlations coming from protons are more or less the same, as expected.

In Table III, the spin-isospin two-nucleon channels involved for each component of the Gogny force are recalled (crosses), and circles indicate the channels and components contributing to the correlation part of the wave function in Eq. (38). The spin-orbit contributes to the $(S = 1, T = 1)$ channel, and the density-dependent term acts only in the mean-field part. The residual interaction coming from the two Gaussians arises in both $(S = 0, T = 1)$ and $(S = 1, T = 1)$ channels [6].

Because our method of solving the configuration mixing equations does not allow us to extract the contribution of each term to the correlation energy, we have studied the influence of these different terms on the correlation content of the wave function by removing them selectively from the residual part of the nuclear Hamiltonian.

First, removing the Coulomb contribution from the residual part of the Hamiltonian changes the correlation energies of the second column in Table II for ^{100}Sn, ^{106}Sn, and ^{116}Sn to 2.98, 3.92, and 4.68 MeV, respectively; that is, the correlation energy decreases by $\simeq$700 keV in all three isotopes.

TABLE III. Spin-isospin ST channels present in each component of the Gogny force (crosses). The circles indicate the channels and components that contribute to the residual interaction taken into account by the correlated wave functions defined in Eq. (38).

S, T	$S = 0$, $T = 1$	$S = 1$, $T = 1$	$S = 0$, $T = 0$	$S = 1$, $T = 0$
Central	$\otimes$	$\otimes$	$\times$	$\times$
Density				$\times$
Spin-orbit		$\otimes$		
Coulomb	$\otimes$	$\otimes$		

TABLE IV. Wave-function components, in percentage, for ^{116}Sn, ^{106}Sn, and ^{100}Sn.

Nucleus	$T(0,0)$	$T(0,1)$	$T(1,0)$	$T(0,2)$	$T(1,1)$	$T(2,0)$
^{116}Sn	65.38	26.04	4.50	2.68	1.23	0.17
^{106}Sn	67.44	25.29	3.63	2.54	0.99	0.11
^{100}Sn	90.85	5.02	3.70	0.16	0.18	0.09

Second, the different components of the nuclear residual interaction listed in Table III have been successively removed in addition to the Coulomb contribution mentioned above. As a result, removing all components except the singlet even one ($S = 0, T = 1$) leaves the correlation energy practically unchanged, and removing the singlet even residual interaction completely kills the nuclear correlation energy. Hence the main sources of correlations are the ($S = 0, T = 1$) channel of the nuclear force—the one that contributes to pairing correlations in the HFB approach—and the Coulomb interaction between protons.

3. *Structure of correlated wave functions*

To have a measure of the amount of correlations in the mp-mh wave function $|\Psi'\rangle$, we define the quantity $T(i, j)$ as

$$T(i,j) = \sum_{\alpha_\pi \alpha_\nu}^{ij} |A_{\alpha_\pi \alpha_\nu}|^2 = \sum_{\alpha_\pi \alpha_\nu}^{ij} \left|U^p_{\alpha_\pi}\right|^2 \left|U^n_{\alpha_\nu}\right|^2. \qquad (47)$$

The first and second arguments of T stand for the number of proton and neutron excited pairs included in $|\Psi'\rangle$, respectively.

Table IV displays the values obtained for $T(i, j)$ with $0 \leqslant i \leqslant 2$ and $0 \leqslant j \leqslant 2$ for the three Sn isotopes. Using $\sum_{j=0} T(i, j) = 1$, $T(i, j)$ is expressed in percentage. One observes that the HF description is approximate even in ^{100}Sn, since $T(0, 0)$ significantly differs from 100% in this nucleus [$T(0, 0) \simeq 91\%$]. The remaining 9% essentially comes from one-pair excitation in either the proton sector or the neutron one. Two-pair correlations are negligible in this nucleus. As expected, the two superfluid nucleus wave functions contain large contributions from one-pair excitations in the neutron sector ($\simeq$25%) and, to a lesser extent, from one-pair proton excitation ($\simeq$2.5%) and two-pair excitation ($\simeq$3.5–4%).

It is interesting to note that if only one-pair excitations are included in the wave function $|\Psi'\rangle$, significant modifications occur to the above numbers. This is illustrated in Table V. The $T(0, 0)$ coefficients are seen to noticeably increase and the $T(0, 1)$ to strongly decrease, especially in the two superfluid nuclei. This shows that although two-pair configurations have a relatively small weight in the ground state wave function, their presence strongly affects the other components of this wave function. Let us mention that three and higher order pair configurations have no influence on the overall structure of the wave function. Let us add that many one-pair coefficients $|A|^2$ contribute with small and similar magnitudes.

TABLE V. Components of ^{116}Sn, ^{106}Sn, and ^{100}Sn wave functions including only configurations with up to one excited pair.

Nucleus	$T(0,0)$	$T(0,1)$	$T(1,0)$
^{116}Sn	87.21	8.98	3.81
^{106}Sn	88.06	8.95	2.98
^{100}Sn	92.89	3.99	3.12

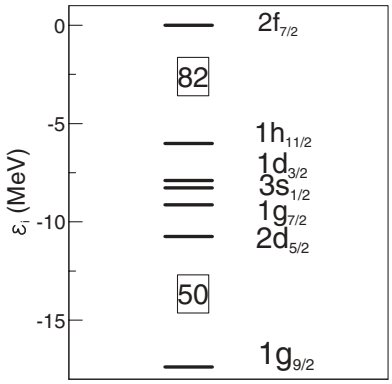

FIG. 4. Neutron single-particle levels in ^{106}Sn.

As can be seen in Table IV, correlations are similar in the ground state description of ^{106}Sn and ^{116}Sn and most part of them come from neutron pairing. As already pointed out, the proton contribution is more or less unchanged from one isotope to the other. The difference between the isotopes essentially comes from the neutron part.

In Fig. 4, a schematic representation of neutron single-particle states pertaining to the 50–82 major shell is drawn.

For ^{106}Sn, the neutron Fermi level is $2d_{5/2}$, and it is completely filled in the HF approximation. The gap between the $2d_{5/2}$ and $1g_{7/2}$ subshells is only 1.5 MeV. The excitation of a neutron pair costs at least $\simeq$3.0 MeV. Note that in BCS or HFB calculations with the D1S Gogny force, pairing switches on when the energy gap between the last occupied and the first unoccupied level is of the order of $\simeq$3.5 MeV. One obtains a depletion of the $T(0, 0)$ component essentially in favor of the $T(0, 1)$ component, which is much larger in ^{106}Sn ($\simeq$25.29%) than in ^{100}Sn ($\simeq$5.02%). The coupling between the configurations corresponding to the excitation of $2d_{5/2}$ neutron pairs to the $1g_{7/2}$ subshell and the HF configuration is relatively strong. Those 12 configurations constitute $\simeq$15.5% of the total wave function. The three configurations corresponding to excitation of $2d_{5/2}$ neutron pairs to the $3s_{1/2}$ subshell account for $\simeq$1% of the total wave function and the six configurations corresponding to excitation of $2d_{5/2}$ neutron pairs in the $1d_{3/2}$ subshell for $\simeq$3%. All the other configurations ($\sim 70 \times 10^6$ as indicated in Table I) each contribute extremely small amounts.

In ^{116}Sn, the $T(0, 1)$ component is even larger than the ^{106}Sn one. The neutron Fermi level is the completely filled $3s_{1/2}$ subshell. As can be seen on Fig. 4, the $1d_{3/2}$ subshell is very close to the $3s_{1/2}$ one: the gap is $\simeq$300 keV. The lowest pair excitation energy is much smaller than in ^{106}Sn: $\simeq$600 keV. However, the $T(0, 1)$ component of ^{116}Sn is close to the ^{106}Sn one. This comes from the fact that the larger energy

gap in ^{106}Sn is compensated for by the larger degeneracy of the $1g_{7/2}$ state compared to the $3s_{1/2}$ one.

Calculations for ^{116}Sn involve a total number of configurations of $\sim 81 \times 10^6$. As for ^{106}Sn, one can isolate a few configurations with strong weights. (i) The two configurations corresponding to the excitation of the $3s_{1/2}$ neutron pair into the $1d_{3/2}$ subshell account for 8.2% of the total wave function. (ii) The six configurations corresponding to the excitation of the $3s_{1/2}$ neutron pair into the $1h_{11/2}$ subshell total 2.5%. (iii) Sixty-seven configurations, most of them being of the one excited pair type, have individual weights larger than 0.05% and a summed contribution of 12.5%.

In the ^{106}Sn and ^{116}Sn wave functions, the two excited pair configurations are more important than in ^{100}Sn, more particularly $T(0, 2)$ and $T(1, 1)$, which are equal to $\simeq$2.6% and $\sim$1%, respectively. Comparisons of Table IV and Table V for ^{106}Sn and ^{116}Sn are clearly consistent with this result, as the $T(0, 0)$ and $T(0, 1)$ components are strongly affected by the removal of the two excited neutron pair configurations. One sees that there is a strong coupling on the one hand between HF and one excited neutron pair configurations and, on the other hand between one and two excited neutron pair configurations. The $T(2, 0)$ component appears negligible for the description of the three Sn ground states.

To conclude this section, let us discuss the separate proton and neutron contributions to the correlated wave function of ^{106}Sn, the nucleus having the most correlated ground state. As proton-neutron pairing is not taken into account, the $T(i, j)$ quantities decompose into the product of a proton and a neutron contribution:

$$T(0,0) = \left|U^p_\pi\right|^2 \cdot \left|U^n_\nu\right|^2 = T^\pi_0 \cdot T^\nu_0, \tag{48}$$

$$T(0,1) = \left|U^p_\pi\right|^2 \cdot \sum_{\alpha_\nu}^{i=0,j=1} \left|U^n_{\alpha_\nu}\right|^2 = T^\pi_0 \cdot T^\nu_1,$$

$$T(1,0) = \left|U^n_\nu\right|^2 \cdot \sum_{\alpha_\pi}^{i=1,j=0} \left|U^p_{\alpha_\pi}\right|^2 = T^\nu_0 \cdot T^\pi_1, \tag{49}$$

$$T(0,2) = \left|U^p_\pi\right|^2 \cdot \sum_{\alpha_\nu}^{i=0,j=2} \left|U^n_{\alpha_\nu}\right|^2 = T^\pi_0 \cdot T^\nu_2,$$

$$T(2,0) = \left|U^n_\nu\right|^2 \cdot \sum_{\alpha_\pi}^{i=2,j=0} \left|U^p_{\alpha_\pi}\right|^2 = T^\nu_0 \cdot T^\pi_2. \tag{50}$$

Numerical calculations in ^{116}Sn give:

$$\begin{aligned} T^\pi_0 &\simeq 93\%, \quad T^\pi_1 \simeq 6\%, \quad T^\pi_2 \simeq 0\%, \\ T^\nu_0 &\simeq 70\%, \quad T^\nu_1 \simeq 28\%, \quad T^\nu_2 \simeq 3\%. \end{aligned} \tag{51}$$

One sees that for this nucleus, even though $T(0, 0) \simeq 65\%$, neutron mean values of observables will be much more affected by correlations than proton ones.

C. Self-consistency effect

In this section, we study the effect of self-consistency on quantities such as correlation energy, components of correlated wave function, single-particle spectra, and single-particle occupation probabilities. We also look at nuclear radii (neutron skin and charge radii) and first 0^+ excited states, for which experimental data are available for most of the Sn isotopes. When possible, comparisons with BCS or HFB approaches will be done. As explained in Sec. II, the full solution of mp-mh equations consists of solving the system of Eqs. (8) and (20). However, as mentioned earlier [in the paragraph following Eq. (33)], instead of solving Eq. (20), we have used an approximate procedure consisting of diagonalizing $h[\rho]$ and have ignored the contribution of σ to $h[\rho]$.

TABLE VI. Correlation energy as defined in the text for ^{116}Sn, ^{106}Sn, and ^{100}Sn. The mp-mh correlated wave functions including configurations with up to two excited pairs. Energies are expressed in MeV.

Nucleus	$\lvert E^{\text{with}}_{\text{corr}}\rvert$	$\lvert E^{\text{without}}_{\text{corr}}\rvert$	$\lvert E^{\text{BCS}}_{\text{corr}}\rvert$	$\lvert E^{\text{HFB}}_{\text{corr}}\rvert$
^{116}Sn	4.75	3.45	3.25	3.86
^{106}Sn	4.09	3.54	1.37	1.73
^{100}Sn	3.19	2.79	0.00	0.00

All the following self-consistent results have been obtained using truncated proton and neutron single-particle spaces, including the 98 lowest proton single-particle levels and the 141 lowest neutron single-particle levels. The total number of configurations is of the order of 10×10^6 for ^{116}Sn, 9×10^6 for ^{106}Sn, and 8×10^6 for ^{100}Sn. Note that these numbers are significantly smaller than those of Sec. III B, where 286 doubly degenerate single-particle levels were used for protons or neutrons.

1. *Self-consistent correlation energy*

In this section, we discuss the effect of the truncation of the single-particle space and the role of self-consistency on the correlation energy. Results are presented in Table VI for the four cases: mp-mh configuration mixing approach with and without self-consistency denoted $E^{\text{with}}_{\text{corr}}$ and $E^{\text{without}}_{\text{corr}}$, BCS and HFB approaches labeled, respectively, $E^{\text{BCS}}_{\text{corr}}$ and $E^{\text{HFB}}_{\text{corr}}$. Let us note that the values indicated for BCS and HFB approximations are deduced from self-consistent calculations that include the full single-particle space associated with 11 shell harmonic oscillator bases (286 doubly degenerate levels). The BCS approximation is defined here as the reduction of the HFB approach in which only the elements of the pairing field matrix that are diagonal in the representation that diagonalizes the one-body Hamiltonian $h[\rho]$ are taken into account [31]. These diagonal terms therefore are obtained from the full Gogny interaction. The mp-mh correlated wave functions include configurations built with one and two excited pairs, as discussed in the Sec. III B.

By comparing $E^{\text{without}}_{\text{corr}}$ of Table VI and $E^{\text{total}}_{\text{corr}}$ of Table II, one observes that truncating the proton and neutron single-particle spaces has a quantitative effect on the total correlation energy, especially in the case of ^{116}Sn. The reason is that high-energy configurations are so numerous that even though they have very small individual contributions, in the end, they bring a nonnegligible additional energy.

TABLE VII. Wave-function components, in percentage, for ^{116}Sn, ^{106}Sn, and ^{100}Sn. Results are deduced from truncated proton and neutron single-particle spaces without self-consistency.

Nucleus	$T(0,0)$	$T(0,1)$	$T(1,0)$	$T(0,2)$	$T(1,1)$	$T(2,0)$
^{116}Sn	65.06	26.49	4.22	2.87	1.21	0.15
^{106}Sn	67.57	26.00	2.71	2.84	0.81	0.07
^{100}Sn	91.05	4.98	3.55	0.17	0.17	0.08

Table VII shows the components of correlated wave functions for proton and neutron truncated single-particle spaces without self-consistency. Comparing these values with those of Table IV, one sees that wave-function contents are very similar (differences are less than 0.3%).

From Table VI, one sees that, comparing $E_{\rm corr}^{\rm with}$ and $E_{\rm corr}^{\rm without}$, self-consistency brings an additional energy of the order of 400–500 keV for ^{100}Sn and ^{106}Sn. For ^{116}Sn, one obtains a correlation energy larger by $\simeq$1.3 MeV. We will go back to this point in the next section. Moreover, even with smaller single-particle spaces, the mp-mh configuration mixing approach provides systematically more correlations than the BCS or HFB approaches (HFB usually gives more pairing correlations than BCS).

The difference between $E_{\rm corr}^{\rm with}$ and $E_{\rm corr}^{\rm HFB}$ is around $\simeq$0.9 MeV for ^{116}Sn, $\simeq$2.3 MeV for ^{106}Sn, and $\simeq$3.2 MeV for ^{100}Sn. The latter case is the most striking, because neither BCS nor HFB are able to find correlations in this nucleus. As correlations coming from protons are quantitatively the same in the three Sn isotopes, this is a confirmation of the known idea that BCS or HFB approaches are good approximations in strong pairing regimes but fail for weak pairing regimes.

2. *Structure of self-consistent correlated wave functions*

We present in Table VIII wave-function components (in percentage) obtained from self-consistent calculations. Comparing with Table VII, $T(0,0)$ has decreased by $\simeq$3%. In the case of ^{100}Sn, this decrease is counterbalanced by an increase of $T(0,1)$ and $T(1,0)$. This is partly due to a small reduction of proton ($\simeq$300 keV) and neutron ($\simeq$50 keV) gaps between the $2g_{9/2}$ and $2d_{5/2}$ single-particle levels. The HF proton and neutron gaps between these two levels are, respectively, $\simeq$6.88 and $\simeq$6.73 MeV.

For ^{106}Sn, the effect is a little more pronounced, as it is accompanied by a $\simeq$5% reduction of $T(0,0)$. As we will discuss later, we observe a $\simeq$300 keV reduction of the proton gap between $2g_{9/2}$ and $2d_{5/2}$ and a $\simeq$70 keV reduction of the neutron gap between $2d_{5/2}$ and $1g_{7/2}$. The HF proton and neutron gaps between the single-particle levels mentioned just before are, respectively, $\simeq$6.21 and $\simeq$1.86 MeV.

TABLE VIII. Components of self-consistent correlated wave functions for ^{116}Sn, ^{106}Sn, and ^{100}Sn, including configurations with up to two-pair excitation. Components are expressed in percentage.

Nucleus	$T(0,0)$	$T(0,1)$	$T(1,0)$	$T(0,2)$	$T(1,1)$	$T(2,0)$
^{116}Sn	42.09	44.28	3.00	8.43	2.09	0.11
^{106}Sn	62.90	28.65	3.54	3.62	1.17	0.11
^{100}Sn	88.19	6.36	4.74	0.27	0.29	0.15

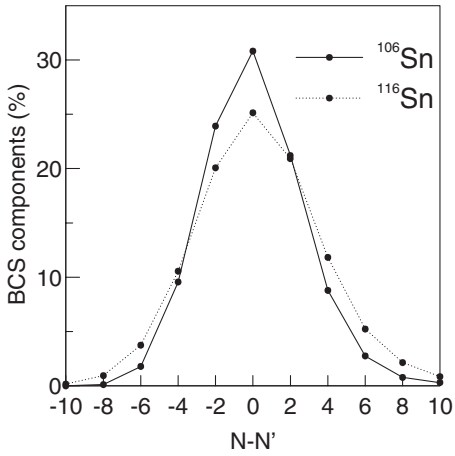

FIG. 5. Distribution of neutron number components of the BCS wave functions of ^{106}Sn and ^{116}Sn.

For ^{116}Sn, the most surprising effect is the large depletion of the $T(0,0)$ component. The $T(0,1)$ component is now the largest one: $\simeq$44% vs $\simeq$42% for $T(0,0)$. We observe also an appreciable jump of the $T(0,2)$ component. As we will analyze later in more detail, this effect is essentially explained by the rearrangement of neutron single-particle levels. Here again, the reason is the neutron reduction of gaps between $3s_{1/2}$ and $2d_{3/2}$ and $2d_{3/2}$ and $1h_{11/2}$ subshells. Consequently, the rearrangement of neutron single-particle states due to self-consistency has produced (i) a reduction of $\simeq$70 keV of the 630 keV gap between $3s_{1/2}$ and $2d_{3/2}$, and (ii) a reduction of $\simeq$300 keV for the 1.21 MeV gap between $2d_{3/2}$ and $1h_{11/2}$, which is equal to $\simeq$1.21 MeV.

Let us note that changes in single-particle energies are bigger in ^{116}Sn because the implied gaps are smaller.

In the following, we compare mp-mh and PBCS wave functions. We make use of Eq. (36), which gives a formal expression for PBCS wave functions. In Fig. 5, the decomposition of BCS wave functions according to the difference $N - N'$, where N' is the nucleus neutron number, is shown for ^{106}Sn and ^{116}Sn. ^{100}Sn has not been considered, since the BCS solution is identical to the HF solution. For ^{106}Sn and ^{116}Sn, the neutron BCS wave functions spread essentially on 11 values of $N - N'$. The particle number squared fluctuation $(\Delta N)^2 = {}_\nu\langle BCS|\hat{N}^2|BCS\rangle_\nu - N^2 = 4\sum_{k>0} u_k^2 v_k^2$ is 6.71 for ^{106}Sn and 9.95 for ^{116}Sn. It is larger for ^{116}Sn than for ^{106}Sn because pairing correlations are stronger in ^{116}Sn.

The main component of BCS wave functions in both nuclei has the good particle number $N - N' = 0$. It represents $\simeq$31% and $\simeq$25% of the total BCS wave function, respectively. The components $N - N' = \pm 2$ are of the order of 20%, and the components $N - N' = \pm 4 \simeq 10\%$. For ^{106}Sn, the last nonnegligible components are the $N - N' = \pm 6$ ones, with percentages around 2%. For ^{116}Sn, the $N - N' = \pm 6$ components are larger and contribute $\simeq$5%, whereas the $N - N' = \pm 8$ components are quite small ($\simeq$0.2%).

TABLE IX. Components of ^{106}Sn and ^{116}Sn PBCS after variation wave function. Components are expressed in percentage.

Nucleus	$T(0,0)$	$T(0,1)$	$T(0,2)$	$T(0,3)$	$T(0,4)$
^{106}Sn	29.09	54.78	15.88	0.25	∼0
^{116}Sn	8.03	43.75	38.55	9.67	∼0

We now look at the decomposition of the component having the good particle number in terms of configurations characterized by a given number of excited pairs [see Eq. (36)]. To compare this decomposition with the mp-mh wave function, we have normalized this component to unity. Results are reported in Table IX. By comparing with the results of Table VII, one sees that for both ^{106}Sn and ^{116}Sn, the content of the PBCS after the variation wave function is strongly different from the one of the mp-mh wave function. The $T(0,0)$ component is only $\simeq$29% for ^{106}Sn and $\simeq$8% for ^{116}Sn. This means that the PBCS wave function overestimates the contribution of excited configurations.

To better understand these results, we compared the single-particle levels obtained in the three approaches HF, BCS, and mp-mh. To this end, we expressed the BCS single-particle states $|i_{\rm BCS}\rangle$ and the mp-mh ones $|i_{\rm mp-mh}\rangle$ as linear combinations of the HF single-particle states $|i_{\rm HF}\rangle$. For ^{106}Sn and ^{116}Sn, we determined that each BCS or mp-mh single-particle state overlaps with the corresponding HF state by 99.999%. This means that HF, BCS, and mp-mh single-particle states are very similar. The spherical single-particle states with given quantum numbers do not mix between themselves under the effect of pairing correlations. Consequently, components of PBCS wave functions depend only on the values of the variational parameters v_n and u_n. The difference between the $T(i,j)$ components of PBCS and mp-mh wave function appears as a consequence of the well-known fact that BCS overestimates pairing correlations [28], whereas mp-mh wave functions are much closer to the exact ones [16].

3. *Single-particle spectra and occupation probabilities in the self-consistent mp-mh approach*

It is well known that when one goes beyond the HF approximation, the notion of single-particle spectra begins to be lost (except in the BCS approximation). Equation (20) illustrates this idea, as $h[\rho]$ and ρ cannot be simultaneously diagonalized. The same phenomenon occurs also in HFB theory. However, single-particle spectra can be obtained either by diagonalizing the density matrix ρ and taking the mean value of $h[\rho]$ or by diagonalizing $h[\rho]$. Here, the second scheme will be used.

In this section, we are interested in single-particle level shifts due to pairing-type correlations. In the representation that diagonalizes $h[\rho]$ and in the special case of the excited pairs wave function, the one-body density matrix calculated as the mean value of the density operator with respect to the correlated wave function is diagonal. Diagonal terms are directly interpreted as fractional occupation probabilities.

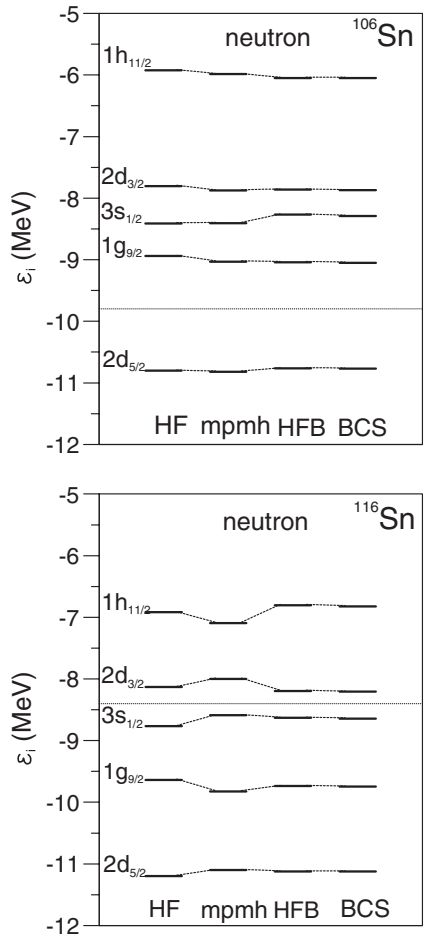

FIG. 6. Neutron single-particle spectra for ^{106}Sn and ^{116}Sn, in the HF, mp-mh, HFB, and BCS approaches. The dotted horizontal line is located between the HF Fermi level and the first empty level.

In Fig. 6, the neutron level of the 50–82 major shell for ^{106}Sn and ^{116}Sn deduced from four approaches (HF, mp-mh configuration mixing, HFB, and BCS) are shown. For the two nuclei, one can note two tendencies: (i) Levels are more compressed in the mp-mh approach than in the HF ones, and (ii) the gap between the HF Fermi level and the next level decreases when pairing correlations are taken into account, the effect being the larger in HFB.

In Fig. 7, all bound proton single-particle levels are presented in the case of ^{116}Sn. ^{100}Sn and ^{106}Sn are very similar. We observe that proton single-particle levels deduced from the mp-mh configuration mixing method are systematically shifted upward. This comes from the well-identified effect of including the Coulomb interaction in the residual interaction responsible for correlations [32]. Besides, we obtained also a small compression of proton spectra as the most shifted levels are the deeper ones.

To interpret in more detail what happens with single-particle spectra, we examine the quantity $\epsilon_{\rm HF} - \epsilon$, where $\epsilon_{\rm HF}$ is the energy of HF single-particle states and ϵ the corresponding energy found in other approaches (mp-mh, HFB, or BCS). Figure 8 displays energy shifts of bound proton and neutron single-particle levels, between the HF and mp-mh configura-

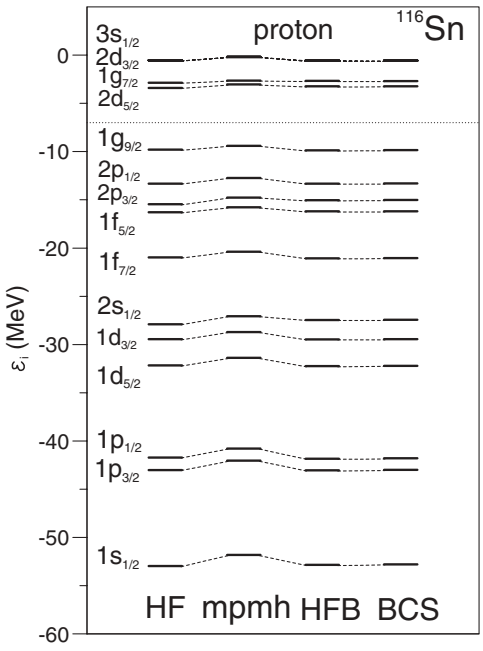

FIG. 7. ^{116}Sn proton single-particle spectra from the HF, mp-mh, and HFB approaches. Only bounded states have been drawn. The dotted horizontal line is between occupied and empty single-particle levels in a pure HF approach.

tion mixing approaches for ^{100}Sn. One observes that proton single-particle states are systematically shifted upward in the mp-mh configuration mixing method. One also sees that this shift decreases when going from the bottom to the top of the potential well. It is $\simeq$1.2 MeV for the $1s_{1/2}$ state and $\simeq$0.5 MeV at the Fermi surface. For neutrons, one obtains a different scenario. First, shifts are smaller (<200 keV) and second shifts become positive above the Fermi surface. This sign inversion produces a small compression of the neutron spectrum. It seems intuitive that, at least, a part of the single-particle levels should be shifted upward when correlations are present, since the mean field that gives minimal total energy is the HF one. The level compression effects may be attributed to the coupling of the particle propagation with mean-field dynamics, whereas the different behavior of protons and neutrons comes from the Coulomb residual interaction.

Let us turn to ^{106}Sn, a nucleus where BCS pairing correlations are relatively small. Figure 9 presents the single-particle energy shifts obtained from the mp-mh, HFB, and BCS approaches, together with the mp-mh shifts in ^{100}Sn taken from Fig. 8 (stars). For protons, the mp-mh configuration mixing method predicts systematic upward shifts of the same order of magnitude or larger (for the $1s_{1/2}$ state) than those of ^{100}Sn. The proton shifts obtained in ^{106}Sn by the mp-mh approach appear to originate from two effects: the influence of the same kind of correlations as in ^{100}Sn and the effect of neutron pairing. The differences with ^{100}Sn can be explained by the sign of the coupling associated with pairing correlations. For example, the $1s_{1/2}$ proton shifts found in the mp-mh approach for ^{100}Sn and the HFB one for ^{106}Sn have the same sign, so the total $1s_{1/2}$ shift in ^{106}Sn is larger than the ^{100}Sn one. On the contrary, the $1f_{5/2}$ proton shifts found in the mp-mh approach for ^{100}Sn and the

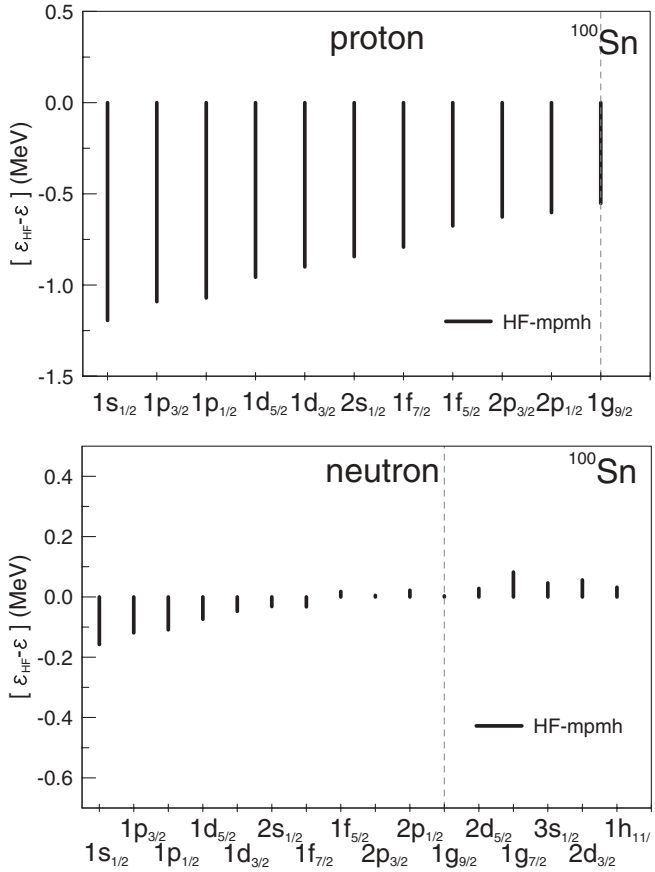

FIG. 8. ^{100}Sn proton and neutron single-particle level energy differences $\epsilon_{\rm HF} - \epsilon$ between HF and mp-mh approaches. Energies are expressed in MeV. The vertical dashed line represents the Fermi level. Only bound levels have been drawn.

HFB approach for ^{106}Sn have opposite signs. Consequently, the final proton shift in ^{106}Sn is reduced in comparison with the ^{100}Sn one. For neutrons, a similar behavior is obtained. However, shifts are smaller, and they appear essentially in s and p single-particle states.

Figure 10 displays energy shifts obtained in ^{116}Sn. Similar conclusions to those of ^{106}Sn can be drawn, except for the $2d_{3/2}$ and $1h_{11/2}$ neutron orbitals, which tend to be closer to each other in the mp-mh configuration mixing approach. Besides, for this nucleus, an inversion between the neutron $1f_{5/2}$ and $2p_{3/2}$ states has been obtained with mp-mh as well as with HFB or BCS approaches. The HFB approximation tends to amplify this inversion by about $\simeq$300 keV in comparison with the mp-mh configuration mixing method.

In the mechanism of adding the two previously mentioned effects (^{100}Sn type correlations and pairing), the total HFB or BCS shifts found for ^{106}Sn and ^{116}Sn and those found in ^{100}Sn do not give exactly the shifts obtained in the mp-mh configuration mixing for ^{106}Sn and ^{116}Sn but only the main trend. However, one must point out that the structure of orbitals is expected to change from one isotope to the other one.

The influence of the residual interaction can be measured also through the values of the single-particle states occupation:

$$v_{\tau i}^2 = \langle \Psi | a_{\tau i}^+ a_{\tau i} | \Psi \rangle, \tag{52}$$

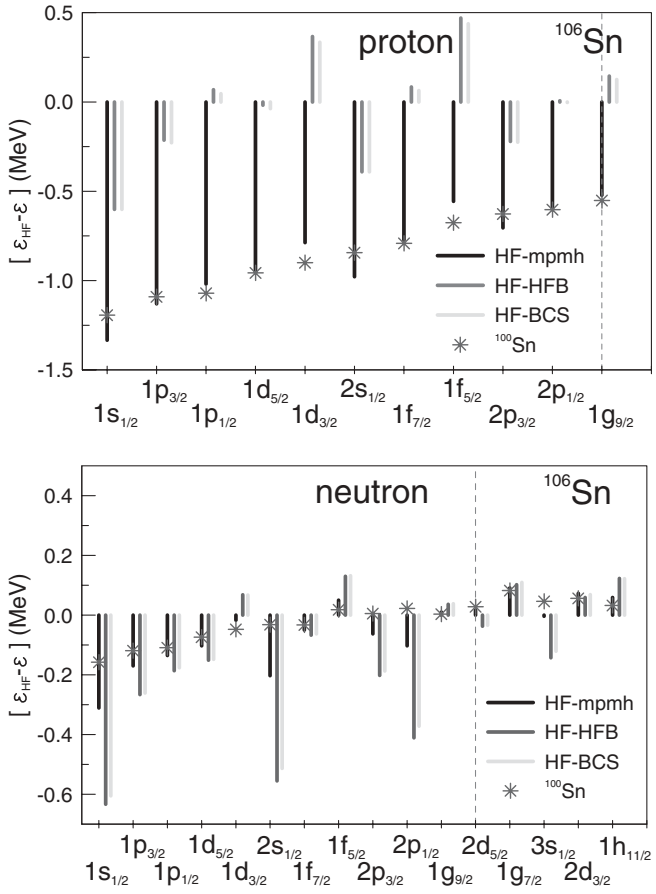

FIG. 9. Same as Fig. 8, but for ^{106}Sn. The stars indicate the values obtained in ^{100}Sn from the mp-mh approach. The vertical lines indicate the results from HF, mp-mh, HFB, and BCS approaches.

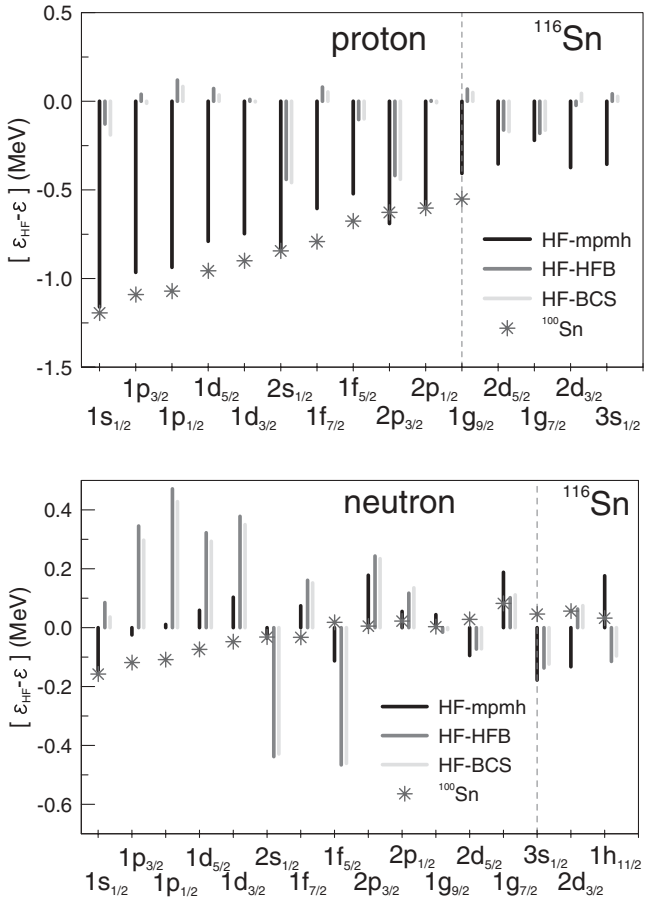

FIG. 10. Same as Fig. 8, but for ^{116}Sn.

where $|\Psi\rangle$ represents here the ground state wave function for a given approximation (HF+BCS, HFB, mp-mh configuration mixing).

In Fig. 11, neutron occupation probabilities for single-particle states located around the Fermi surface are drawn for ^{100}Sn, ^{106}Sn, and ^{116}Sn. They have been calculated for five different cases: non-self-consistent mp-mh configuration mixing (cross), self-consistent mp-mh configuration mixing (star), HFB (circle), PBCS (triangle), and BCS (diamond) approaches.

In ^{100}Sn, HFB, PBCS, and BCS give the trivial HF zero or one occupation probabilities. In the mp-mh configuration mixing approaches (non-self-consistent or self-consistent), neutron occupation probabilities are no longer equal to 0 or 1, but they are still close to these values. Let us note that a similar behavior is obtained for protons in all three Sn isotopes calculated with the mp-mh configuration mixing description. Referring to the discussion about the structure of correlated wave functions in Sec. III B3, neutron correlations can be estimated to be less than 10% of the neutron correlated wave function in ^{100}Sn. Proton correlations in ^{100}Sn as well as in ^{106}Sn and ^{116}Sn also represent less than 10%. This explains why occupation probabilities, in those cases, are so close to the HF ones.

In ^{106}Sn and ^{116}Sn, occupation probabilities for neutron are markedly different. A pronounced depletion of the single-particle states below the Fermi level is obtained, which is compensated for by a non-zero population of single-particle states above the Fermi sea. The results in Fig. 11 show that HFB, PBCS, and BCS overestimate the occupation probabilities above the Fermi sea and underestimate those within the Fermi sea in comparison to the mp-mh configuration mixing method. A similar behavior has been observed when comparing HFB, PBCS, and BCS with the results of the exactly solvable model of Richardson [16,28]. To conclude, one observes that when pairing correlations are medium (^{106}Sn) or weak (^{100}Sn), self-consistent, and non-self-consistent mp-mh configuration mixing calculations give similar results. In contrast, in a strong pairing regime (^{116}Sn), self-consistent mp-mh calculations give results significantly different from those of non-self-consistent ones. Self-consistence induces a stronger depletion of single-particle states inside the Fermi sea, which, however, is smaller than the one obtained with HFB.

4. Radii

The size and shape of nuclei strongly depend on the number of protons and neutrons and, to a lesser extent, on the magnitude of correlations present in the internal structure.

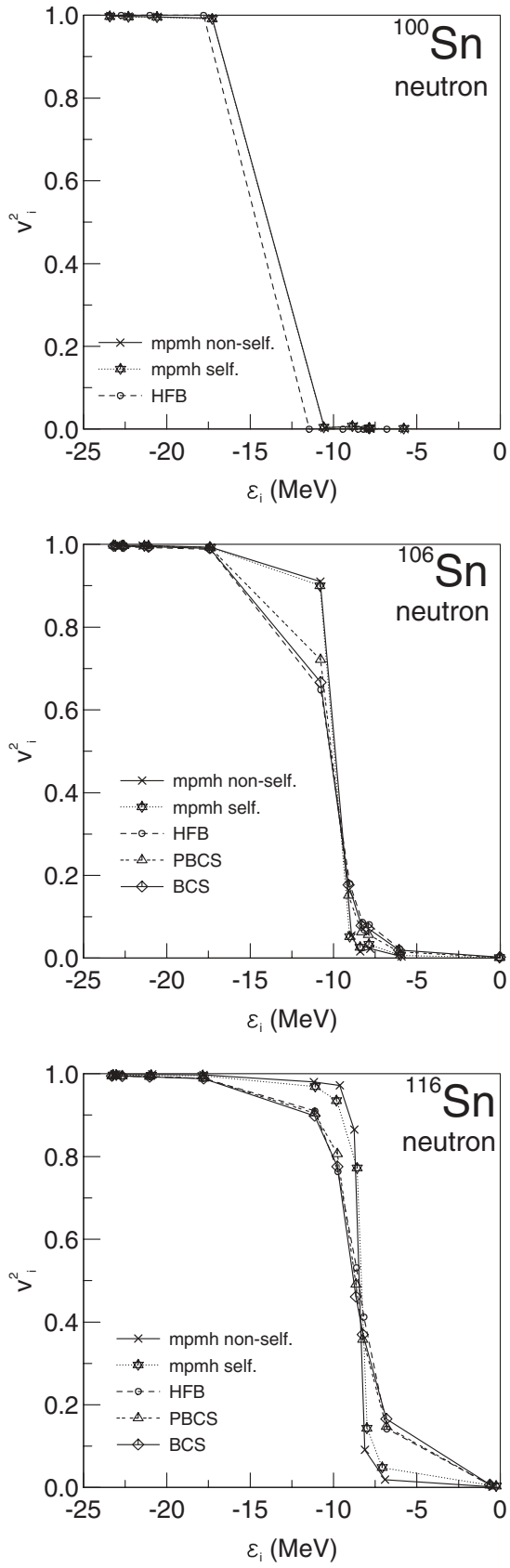

FIG. 11. Neutron single-particle occupation probabilities as functions of single-particle levels energies in ^{116}Sn, ^{106}Sn, and ^{100}Sn calculated for five different cases (see legend).

The three Sn isotopes studied in this work are found to be spherical with the mp-mh approach. Concerning their size, we have calculated different types of radii and some associated quantities directly comparable with experimental data in order to see the effect of pairing correlations obtained in the particle number conserving mp-mh approach. The total root mean square (rms) radius is

$$r_{av} = \sqrt{\frac{r_p^2 + r_n^2}{Z+N}}, \tag{53}$$

with proton and neutron rms radii defined as

$$r_p = \sqrt{\frac{\int d^3r\, \rho_\pi(r) r^2}{Z}}, \quad r_n = \sqrt{\frac{\int d^3r\, \rho_\nu(r) r^2}{N}}, \tag{54}$$

where $\rho_\pi(r)$ and $\rho_\nu(r)$ are the proton and neutron radial densities. The difference is expressed as

$$\Delta r_{np} = r_n - r_p, \tag{55}$$

a measure of the neutron-skin thickness. The rms charge radius is

$$r_c = \left[r_p^2 + \frac{3}{2}(B^2 - b) - 0.1161 \frac{N}{Z} \right]^{1/2}, \tag{56}$$

where $B = 0.7144$ fm comes from the proton form factor, and b is a correction for the center of mass motion. Assuming a pure harmonic oscillator wave function, b is given by the relation $b = 41.47/\hbar\omega(Z+N)$, where the size parameter $\hbar\omega$ is determined by Bethe's formula $\hbar\omega = 1.85 + 35.5(Z+N)^{-1/3}$ [25]. The third contribution to r_c in Eq. (56) is a correction associated with neutron electromagnetic properties.

The total rms radius r_{av} has been calculated in HF, HFB, and mp-mh approaches for six Sn isotopes (^{100}Sn, ^{106}Sn, ^{114}Sn, ^{116}Sn, ^{120}Sn, and ^{132}Sn). Results are shown in Fig. 12. One observes a regular increase of r_{av} with the mass number A. Values obtained from HF, HFB, and mp-mh approaches are very close to each other, the largest difference being found in

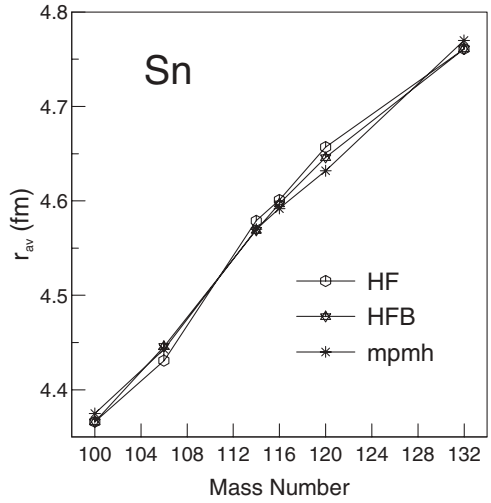

FIG. 12. Total rms radii r_{av} for six Sn isotopes calculated with the HF, HFB, and mp-mh approaches. Lines between points are drawn to guide eye.

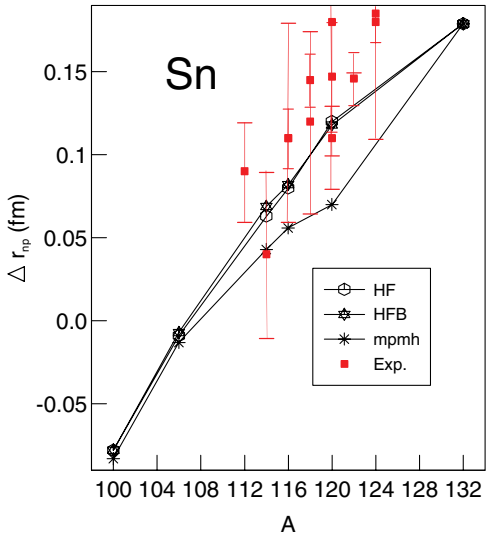

FIG. 13. (Color online) Difference between neutron and proton rms radii Δr_{np} calculated with the HF, HFB, and mp-mh approaches. Experimental measurements with error bars are also represented.

^{120}Sn. This almost regular increase is also obtained in the separate proton and neutron rms radii r_p and r_n. Looking into more detail, one observes that for Sn isotopes containing large pairing correlations, r_{av} is larger in HF than in HFB or mp-mh. The same observation is true also for r_p and r_n taken individually. This result is not very intuitive, as pairing correlation populates levels above the Fermi level having on the average larger spatial extensions. However, this behavior can be explained from the fact that, as shown previously, correlations tend to shift single-particle states downward, hence producing a reduction of single-particle orbital rms radii.

One experimentally accessible quantity is the neutron-proton difference Δr_{np} defined in Eq. (55). This difference gives crucial indications about the distributions of protons and neutrons in nuclei. For that reason, it is a quantity more sensitive to models than the total rms radius r_{av}. Results are displayed in Fig. 13 for six different Sn isotopes. Experimental data have been taken from Refs. [33–36]. In the two light proton rich isotopes ^{100}Sn and ^{106}Sn, where no experimental data are available, the three theoretical approaches give negative values of Δr_{np} very close to each other. The fact that the proton radii are larger than neutron ones is of course due to the magnitude of the Coulomb field in these nuclei. In the heavier Sn isotopes, Δr_{np} changes sign, which means that a neutron skin develops. One observes that the mp-mh approach yields values of Δr_{np} smaller than HF and HFB, especially in the most superfluid nuclei ^{114,116,120}Sn. All calculated values are within experimental error bars, except for the mp-mh configuration mixing calculation of ^{120}Sn and to a lesser extent ^{116}Sn. The low values obtained in midshell Sn with mp-mh configuration mixing mainly come from the large downward shift of the neutron $1h_{11/2}$ orbital (see Fig. 10), which gives rise to a smaller value of the neutron $1h_{11/2}$ orbital radius. One notes that the experimental error bars are quite large and that the different experimental results are scattered over a relatively large range of values.

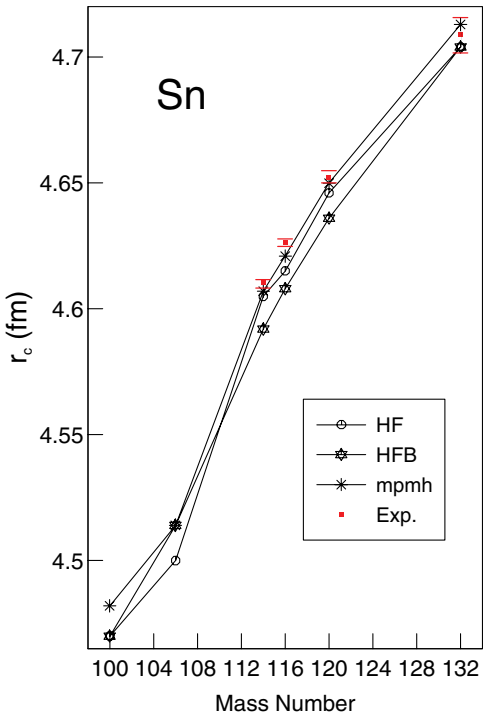

FIG. 14. (Color online) Charge radii for several Sn isotopes calculated within HF, HFB, and mp-mh approaches. Experimental data are indicated by solid squares, with error bars.

To have a more precise idea of the meaning of results concerning Δr_{np}, we have evaluated also the rms charge radius r_c using formula (56). For a given nucleus, r_c depends essentially on r_p. Then, r_c gives an indication of the reliability of r_p calculations. Figure 14 displays the evolution of r_c for the same Sn isotopes as in Fig. 13. Experimental data have been extracted from Refs. [37–40].

One sees that the mp-mh configuration mixing approach gives a description of charge radii closer to experimental values, particularly in isotopes where pairing is large. From this result, one infers that the larger deviations from experiment obtained for Δr_{np} with the mp-mh approach come mainly from the neutron rms radius. It is interesting to note that although the HF and HFB Δr_{np} are closer to experiment, the separate reproduction of r_c, and therefore of r_p and r_n, is not as good as the one obtained with the mp-mh approach.

5. *First excited* 0^+ *state*

Sn isotopes manifest a very rich and complex spectroscopy. In the last two decades, many experiments have been carried out so that a lot of experimental data are now available for most Sn isotopes between $A = 108$ and $A = 132$, giving us the opportunity to study nuclear property changes over a large-range neutron-proton asymmetry. Of course, a complete description of the low-energy spectroscopy of these nuclei is beyond the scope of this work, since it would require taking into account more general correlations than pairing.

Excited 0^+ states have been observed in most Sn isotopes. In this study, we look first at excited 0^+ states and compare their

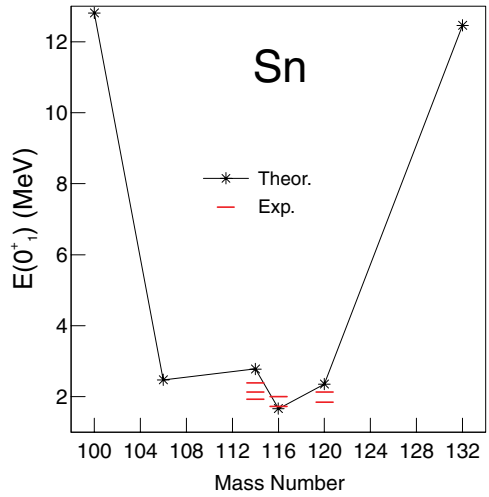

FIG. 15. (Color online) First excited 0+ states calculated with the mp-mh approach for six Sn isotopes. Experimental data for 0^+ are indicated by horizontal bars.

energy to experimental measurements. In Fig. 15, the energy of the first excited 0^+ state calculated using mp-mh configuration mixing is displayed for ^{100}Sn, ^{106}Sn, ^{114}Sn, ^{116}Sn, ^{120}Sn, and ^{132}Sn. Energies vary from $\simeq$12 MeV for the two doubly magic isotopes ^{100}Sn and ^{132}Sn down to $\simeq$2 MeV for midshell isotopes. Among the selected isotopes, experimental data on excited 0^+ energies can be found in the literature only for ^{114}Sn, ^{116}Sn, and ^{120}Sn [41]. They are represented in Fig. 15 by horizontal red bars. The first excited 0^+_1 state in ^{116}Sn is known to be a collective state (it is the head of a rotational band), contrary to the second experimental excited 0^+_2 state [42]. Therefore, a description of the 0^+_1 experimental state is beyond the scope of this work, and the first excited state obtained with the mp-mh approach is likely to be the second experimental 0^+_2 excited state. This point has been stressed in Ref. [43]. With this hypothesis, the difference between experimental and theoretical excitation energies is $\simeq$300 keV in the three isotopes where experimental data are available. One must note that for ^{120}Sn, there is no evidence that the experimental first 0^+_1 excited state is a collective nature, as in ^{116}Sn [43]. Hence, it may be that the first 0^+ state we calculate indeed could be interpreted as the first experimental 0^+. For this nucleus, the difference between experimental and theoretical excitation energies is $\simeq$400 keV. For ^{114}Sn, experimental data give no information about the collectivity of excited 0^+ states. The experimental excitation energies of the three first excited 0^+ states are 1.953, 2.156, and 2.421 MeV, whereas the mp-mh configuration mixing calculation gives $\simeq$2.78 MeV.

IV. SUMMARY AND CONCLUSION

In this paper, we have presented the formalism of a variational configuration mixing self-consistent method adapted to nuclear structure. This approach is an extension of the usual mean-field theory, which is able to treat pairing-like, RPA-like, and particle-vibration correlations in a unified way. No inert core is assumed in this approach. In the spirit of the mean-field theory, the same interaction is used to describe both the mean field and the residual part of the effective Hamiltonian. We have applied this formalism to the special case of pairing-like correlation using the finite-range density-dependent Gogny force. Applications to three Sn isotopes characterized by three BCS pairing regimes have been considered: ^{100}Sn (no pairing), ^{106}Sn (weak pairing), and ^{116}Sn (strong pairing).

We have shown that the mp-mh configuration mixing method systematically finds more correlations than BCS, HFB, and projected BCS (PBCS). In the proton sector, a systematic additional energy of the order of 1.7 MeV has been found for the three Sn isotopes mentioned just above. For the neutron sector, we find that in the strong pairing regime, BCS, HFB, or mp-mh approaches provide similar correlation energy; whereas in weak and medium pairing regimes, mp-mh provides many more correlations than BCS or HFB. Moreover, the structure of mp-mh wave functions appears quite different from those of BCS, HFB, and PBCS. The differences manifest themselves in quantities such as occupation probabilities for which BCS, PBCS, or HFB always overestimate the effect of correlations in comparison to the mp-mh configuration mixing method, and also in nuclear rms radii.

Correlation energies have been shown to converge reasonably well using a small number of p-h excitation (up to 4p-4h) and a number of single-particle states extending to $\simeq$100 MeV above the Fermi sea. On the other hand, self-consistency effects, i.e., the influence of the modification of the single-particle states due to correlations has been found important when correlations are strong, e.g., in ^{116}Sn.

Work is in progress to include more general correlations than those considered in this study.

ACKNOWLEDGMENTS

The authors thank D. Gogny for valuable comments and suggestions about this work, H. Goutte for her help on the manuscript, and J.-P. Delaroche for many useful discussions. Most of the calculations were carried out on the Tera10 and CCRT supercomputers of CEA-DAM Ile de France, Bruyères-le-Châtel, France. N.P would like to thank especially Roger Brel for his kind assistance concerning the Tera-10 access.

APPENDIX A: VARIATIONAL PRINCIPLE WITH RESPECT TO THE MIXING COEFFICIENTS

In this Appendix, we derive the secular equation that determines the mixing coefficients $\{A_{\alpha_\pi \alpha_\nu}\}$. Moreover, we will give details concerning the evaluation of N-body matrix elements associated with one-body and two-body operators.

The first condition given by the variational principle, applied to the energy functional $\mathcal{F}$, [see Eqs. (4) and (7)] reads

$$\frac{\partial \mathcal{F}(\Psi)}{\partial A^*_{\alpha_\pi \alpha_\nu}} = 0. \tag{A1}$$

The two-body nuclear Hamiltonian is defined by

$$\hat{H} = \hat{K} + \hat{V}[\rho]. \tag{A2}$$

In Eq. (A2), the Hamiltonian contains a kinetic term $\hat{K}$ (which includes the one-body center of mass correction) and a density-dependent potential term. As a matter of fact, the general formalism developed in this paper can be applied to any two-body interaction, as for instance Skyrme or Gogny effective forces.

Equation (A1) leads to

$$\sum_{\alpha'_\pi \alpha'_\nu} A_{\alpha'_\pi \alpha'_\nu} \Bigg[\langle \phi_{\alpha_\pi} \phi_{\alpha_\nu} | \hat{H}[\rho] | \phi_{\alpha'_\pi} \phi_{\alpha'_\nu} \rangle + \sum_{\alpha_\pi \alpha_\nu} A^*_{\alpha_\pi \alpha_\nu} \langle \phi_{\alpha_\pi} \phi_{\alpha_\nu} | \int \frac{\partial \hat{V}[\rho]}{\partial \rho(\vec{r})} \frac{\partial \rho(\vec{r})}{\partial A^*_{\alpha'_\pi \alpha'_\nu}} d^3 r | \phi_{\alpha'_\pi} \phi_{\alpha'_\nu} \rangle \Bigg], = \lambda A_{\alpha_\pi \alpha_\nu}. \tag{A3}$$

where $\rho(\vec{r})$ is the nucleon density distribution defined in Eq. (6). After some manipulation, Eq. (A3) takes the form

$$\sum_{\alpha'_\pi \alpha'_\nu} \mathcal{H}_{\alpha_\pi \alpha_\nu, \alpha'_\pi \alpha'_\nu} A_{\alpha'_\pi \alpha'_\nu} = \lambda A_{\alpha_\pi \alpha_\nu}, \tag{A4}$$

where the Hamiltonian matrix $\mathcal{H}$ is defined by

$$\mathcal{H}_{\alpha_\pi \alpha_\nu, \alpha'_\pi \alpha'_\nu} = \langle \phi_{\alpha_\pi} \phi_{\alpha_\nu} | \hat{H} + \sum_{mn\tau} \Re^\tau_{mn} a^+_{\tau m} a_{\tau n} | \phi_{\alpha'_\pi} \phi_{\alpha'_\nu} \rangle, \tag{A5}$$

with $\Re$ a one-body rearrangement field whose matrix elements are

$$\Re^\tau_{mn} = \int d^3\vec{r} \varphi^*_{\tau m}(\vec{r}) \varphi_{\tau n}(\vec{r}) \langle \Psi | \frac{\partial \hat{V}}{\partial \rho(\vec{r})} | \Psi \rangle \tag{A6}$$

and

$$\frac{\partial \hat{V}[\rho]}{\partial \rho(\vec{r})} = \frac{1}{4} \sum_{ijkl} \langle ij | \frac{\partial V[\rho]}{\partial \rho(\vec{r})} | \widetilde{kl} \rangle a^+_i a^+_j a_l a_k. \tag{A7}$$

As can be seen from Eq. (A5), $\mathcal{H}$ requires the evaluation of one-body and two-body matrix elements such as $\langle \phi_{\alpha'} | a^+_i a_j | \phi_\alpha \rangle$ and $\langle \phi_{\alpha'} | a^+_i a^+_j a_l a_k | \phi_\alpha \rangle$. To calculate them, excited configurations are written in the form

$$|\phi_\alpha\rangle = \prod_{i=1}^{N} a^+_{\alpha_i} |0\rangle = a^+_{\alpha_1} a^+_{\alpha_2} \ldots a^+_{\alpha_N} |0\rangle, \tag{A8}$$

where N is the number of particles (either proton or neutron) and $|0\rangle$ stands for the particle vacuum. The set of $\{\alpha_i\}$ indices represents orbitals that are occupied in the configuration $|\phi_\alpha\rangle$. To simplify notations, proton and neutron indices have been omitted in Eq. (A8). The same notation will be used in the following.

One assumes that, in Eq. (A8), particle creation operators are ordered, for example, by increasing single-particle energy when one goes from the left to the right. The set of creation and annihilation operators $\{a^+_i, a_i\}$ follows the fermion anticommutation rules:

$$\begin{aligned} [a^+_i, a_j] &= a^+_i a_j + a_j a^+_i = \delta_{ij}, \\ [a^+_i, a^+_j] &= a^+_i a^+_j + a^+_j a^+_i = 0. \end{aligned} \tag{A9}$$

Using relation (A9), it is easy to show that

$$a_j |\phi_\alpha\rangle = \sum_{m=1}^{N} (-)^{m+1} \delta_{j\alpha_m} \prod_{n=1, n\neq m}^{N} a^+_{\alpha_n} |0\rangle. \tag{A10}$$

Then:

$$a^+_i a_j |\phi_\alpha\rangle = \sum_{m=1}^{N} (-)^{m-1} \delta_{j\alpha_m} a^+_i \prod_{n=1, n\neq m}^{N} a^+_{\alpha_n} |0\rangle, \tag{A11}$$

where there remains to order a^+_i within the list of $a^+_{\alpha_n}$ operators. Therefore

$$a^+_i a_j |\phi_\alpha\rangle = \sum_{m=1}^{N} \delta_{j\alpha_m} (-)^{m-1+i'} |\phi^{im}_\alpha\rangle, \tag{A12}$$

with $i' = i - 1$ if $i \leqslant m$, $i' = i$ if $i \geq m$, and $|\phi^{im}_\alpha\rangle$ is the Slater determinant obtained by removing $a^+_{\alpha_m}$ from $|\phi_\alpha\rangle$, adding a^+_i, and ordering the a^+ from left to right. One sees that $\langle \phi_{\alpha'} | a^+_i a_j | \phi_\alpha \rangle$ is nonzero only if $|\phi^{im}_\alpha\rangle$ and $|\phi_{\alpha'}\rangle$ contain the same orbitals.

For a two-body operator, the evaluation of $\langle \phi_{\alpha'} | a^+_i a^+_j a_l a_k | \phi_\alpha \rangle$ is a little more tedious but is done in the same manner. One first obtains

$$a_l a_k |\phi_\alpha\rangle = (1 - \delta_{lk}) \sum_{m=1}^{N} (-)^{m+1} \delta_{k\alpha_m} \times \sum_{n=1, n\neq m}^{N} (-)^{n'+1} \delta_{l\alpha_n} \prod_{r=1, r\neq n\neq m}^{N} a^+_{\alpha_r} |0\rangle, \tag{A13}$$

with $n' = n$ if $l < k$, and $n' = n - 1$ if $l > k$. Then

$$a^+_i a^+_j a_l a_k |\phi_\alpha\rangle = (1 - \delta_{lk})(1 - \delta_{ij}) \times \sum_{m=1}^{N} (-)^{m+1} \delta_{k\alpha_m} \sum_{n=1, n\neq m}^{N} (-)^{n'+1} \delta_{l\alpha_n} \times a^+_i a^+_j \prod_{r=1, r\neq n\neq m}^{N} (1 - \delta_{i\alpha_r})(1 - \delta_{j\alpha_r}) a^+_{\alpha_r} |0\rangle, \tag{A14}$$

or

$$a^+_i a^+_j a_l a_k |\phi_\alpha\rangle = (1 - \delta_{lk})(1 - \delta_{ij}) \sum_{m=1}^{N} (-)^{m+1} \delta_{k\alpha_m} \times \sum_{n=1, n\neq m}^{N} (-)^{n'+1} \delta_{l\alpha_n} (-)^{i'+j'} |\phi^{ijmn}_\alpha\rangle, \tag{A15}$$

where $(-)^{i'}$ and $(-)^{j'}$ are phases. $|\phi^{ijmn}_\alpha\rangle$ is the Slater determinant obtained by removing $a^+_{\alpha_m}$ and $a^+_{\alpha_n}$ from $|\phi_\alpha\rangle$, adding a^+_i and a^+_j, and ordering the a^+ from left to right. The term $\langle \phi_{\alpha'} | a^+_i a^+_j a_l a_k | \phi_\alpha \rangle$ is nonzero only if $|\phi^{ijmn}_\alpha\rangle$ and $|\phi^{\alpha'}\rangle$ containsthe same orbitals. The calculation of the mean value of one-body and two-body operators is straight forward using

formulas (A12) and (A15). Let

$$\hat{\theta}_1 = \sum_{ij} \langle i|\theta_1|j\rangle a_i^+ a_j \tag{A16}$$

be a one-body operator. Using Eq. (A12), one obtains

$$\begin{aligned}\langle\phi_{\alpha'}|\hat{\theta}_1|\phi_\alpha\rangle &= \sum_i \left(\sum_{l=1}^N \delta_{i\alpha_l}\right) \langle i|\theta_1|i\rangle \langle\phi_{\alpha'}|\phi_\alpha\rangle \\ &\quad + \sum_{i\neq j} \sum_{m=1}^N (-)^{m+1} \delta_{j\alpha_m} \langle i|\theta_1|j\rangle \left\langle\phi_{\alpha'}\middle|\phi_\alpha^{im}\right\rangle. \end{aligned} \tag{A17}$$

The first term on the right-hand side of Eq. (A17) gives a diagonal contribution in the multiconfiguration space. It is a mean-field term. The second term is an off-diagonal contribution which is nonzero only if $|\phi_{\alpha'}\rangle = |\phi_\alpha^{im}\rangle$. In this case, the off-diagonal term is proportional to $\langle i|\theta_1|j\rangle$.

Now, let $\hat{\theta}_2$ be a two-body operator:

$$\hat{\theta}_2 = \sum_{ijkl} \langle ij|\theta_2|\widetilde{kl}\rangle a_i^+ a_j^+ a_l a_k. \tag{A18}$$

Using Eq. (A18), the expression of $\langle\phi_{\alpha'}|\hat{\theta}_2|\phi_\alpha\rangle$ contains three different contributions, as shown in Eq. (A19).

$$\begin{aligned}&\langle\phi_{\alpha'}|\hat{\theta}_2|\phi_\alpha\rangle \\ &= \sum_{i<j} \left(\sum_{p=1}^N \delta_{j,\alpha_p} \sum_{q=1,q\neq p}^N \delta_{i,\alpha_q}\right) \langle\phi_{\alpha'}|\phi_\alpha\rangle \langle ij|\theta_2|\widetilde{ij}\rangle \\ &\quad + \sum_{i<j,j\neq k} \sum_k \left(\sum_{p=1}^N (-)^p \delta_{k,\alpha_p} \sum_{q=1,q\neq p}^N \delta_{i,\alpha_q} \left\langle\phi_{\alpha'}\middle|\phi_\alpha^{ijki}\right\rangle\right) \\ &\quad \times \left\langle ij\middle|\theta_2\middle|\widetilde{ki}\right\rangle \\ &\quad + \sum_{i<j,j\neq k\neq l} \sum_l \left(\sum_{p=1}^N \delta_{i,\alpha_p} \sum_{q=1,q\neq p}^N (-)^{q-1} \delta_{l,\alpha_q} \left\langle\phi_{\alpha'}\middle|\phi_\alpha^{ijil}\right\rangle\right) \\ &\quad \times \langle ij|\theta_2|\widetilde{il}\rangle \\ &\quad + \sum_{i<j,i\neq k\neq l} \sum_k \left(\sum_{p=1}^N (-)^{p-1} \delta_{k,\alpha_p} \sum_{q=1,q\neq p}^N \delta_{j,\alpha_q} \left\langle\phi_{\alpha'}\middle|\phi_\alpha^{ijkj}\right\rangle\right) \\ &\quad \times \langle ij|\theta_2|\widetilde{kj}\rangle \\ &\quad + \sum_{i<j,i\neq k\neq l} \sum_l \left(\sum_{p=1}^N \delta_{j,\alpha_p} \sum_{q=1,q\neq p}^N (-)^q \delta_{l,\alpha_q} \left\langle\phi_{\alpha'}\middle|\phi_\alpha^{ijjl}\right\rangle\right) \\ &\quad \times \langle ij|\theta_2|\widetilde{jl}\rangle \\ &\quad + \sum_{i<j,(i,j)\neq k\neq l} \sum_{l<k} \left(\sum_{p=1}^N (-)^{p+1} \delta_{k,\alpha_p} \right. \\ &\quad \left. \times \sum_{q=1,q\neq p}^N (-)^{q+1} \delta_{l,\alpha_q} \left\langle\phi_{\alpha'}\middle|\phi_\alpha^{ijkl}\right\rangle\right) \langle ij|\theta_2|\widetilde{kl}\rangle. \end{aligned} \tag{A19}$$

The first term corresponds to the usual mean-field contribution. The four following terms as well as the last one are of-diagonal contributions in the multiconfiguration space. The four terms couple Slater determinants $|\phi_\alpha\rangle$ and $|\phi_{\alpha'}\rangle$ differing from one particle in one orbital, and the last term couples two Slater determinants that differ from two particles in two different orbitals.

Let us add that the total energy $\mathcal{E}(\Psi)$ of the nucleus is obtained by multiplying Eq. (A4) by $A^*_{\alpha_\pi\alpha_\nu}$ and summing over $\alpha_\pi\alpha_\nu$. Taking into account the relation $\sum_{\alpha_\pi\alpha_\nu} |A_{\alpha_\pi\alpha_\nu}|^2 = 1$, one gets

$$\mathcal{E}(\Psi) = \lambda - \sum_{mn\tau} \Re^\tau_{mn} \langle\Psi|a^+_{\tau m} a_{\tau n}|\Psi\rangle. \tag{A20}$$

APPENDIX B: VARIATIONAL PRINCIPLE WITH RESPECT TO THE SINGLE-PARTICLE ORBITALS

We detail here the derivation of Eq. (20). The starting point is the second condition of system (7) where one assumes fixed mixing coefficients.

$$\frac{\partial \mathcal{F}(\Psi)}{\partial \varphi^*_{\tau j}} = 0. \tag{B1}$$

Using Eq. (4), the variation $\delta\mathcal{F}(\Psi)$ of the energy functional is

$$\begin{aligned}\delta\mathcal{F}(\Psi) &= \langle\delta\Psi|\hat{H} - \lambda|\Psi\rangle + \langle\Psi|\hat{H} - \lambda|\delta\Psi\rangle \\ &\quad + \langle\Psi|\delta\hat{V}[\rho]|\Psi\rangle, \end{aligned} \tag{B2}$$

with

$$\delta\hat{V}[\rho] = \int d^3\vec{r} \frac{\partial\hat{V}[\rho]}{\partial\rho(\vec{r})} \delta\rho(\vec{r}), \tag{B3}$$

and

$$\delta\rho(\vec{r}) = \langle\delta\Psi|\hat{\rho}(\vec{r})|\Psi\rangle + \langle\Psi|\hat{\rho}(\vec{r})|\delta\Psi\rangle. \tag{B4}$$

First, let us note that the variation of $|\Psi\rangle$ with respect to the orbitals a^+_α can be written as

$$|\delta\Psi\rangle = i\hat{S}|\Psi\rangle, \tag{B5}$$

where $\hat{S}$ is an infinitesimal Hermitian one-body operator

$$\hat{S} = \sum_{kl} S_{kl} a^+_k a_l. \tag{B6}$$

In fact, using Thouless's theorem, a variation of the orbitals can be written as

$$a^+_\alpha \to e^{i\hat{S}} a^+_\alpha e^{-i\hat{S}} \sim a^+_\alpha + [i\hat{S}, a^+_\alpha]. \tag{B7}$$

Therefore, any Slater determinant of the form (A8) varies according to

$$|\phi_\alpha\rangle \to e^{i\hat{S}}|\phi_\alpha\rangle \sim (1 + i\hat{S})|\phi_\alpha\rangle, \tag{B8}$$

as $e^{i\hat{S}}|0\rangle = |0\rangle$. Consequently

$$|\Psi\rangle = \sum_\alpha A_\alpha|\phi_\alpha\rangle \to |\Psi\rangle + |\delta\Psi\rangle = \sum_\alpha A_\alpha(1 + i\hat{S})|\phi_\alpha\rangle, \tag{B9}$$

which yields Eq. (B5).

Let us mention that $|\delta\Psi\rangle$ represents a genuine variation of $|\Psi\rangle$ only if $|\Psi\rangle$ belongs to a subspace of the full N-particle

Hilbert space. This is the case here, since $|\Psi\rangle$ is built from a finite set of mp-mh excitations.

Using Eq. (B5), Eq. (B2) can be expressed as

$$\delta\mathcal{F}(\Psi) = i\langle\Psi|\left(\hat{H} - \lambda + \int d^3\vec{r}\langle\Psi|\frac{\partial\hat{V}(\rho)}{\rho(\vec{r})}|\Psi\rangle\hat{\rho}(\vec{r})\right)\hat{S} - \hat{S}\left(\hat{H} - \lambda + \int d^3\vec{r}\langle\Psi|\frac{\partial\hat{V}(\rho)}{\rho(\vec{r})}|\Psi\rangle\hat{\rho}(\vec{r})\right)|\Psi\rangle. \tag{B10}$$

The second condition (7) finally leads to

$$\langle\Psi|\left[\hat{H} + \int d^3\vec{r}\langle\Psi|\frac{\partial\hat{V}[\rho]}{\partial\rho(\vec{r})}|\Psi\rangle\hat{\rho}(\vec{r}), a_k^+ a_l\right]|\Psi\rangle = 0. \tag{B11}$$

Let σ be the two-body correlation matrix defined as

$$\langle\Psi|a_i^+ a_m^+ a_n a_l|\Psi\rangle = \rho_{li}\rho_{nm} - \rho_{lm}\rho_{ni} + \sigma_{il,mn}. \tag{B12}$$

Equation (B11) can be seen to be equivalent to

$$[h[\rho,\sigma],\rho] = G(\sigma), \tag{B13}$$

with

$$G_{kl}(\sigma) = \frac{1}{2}\sum_{imn}\langle im|V[\rho]|kn\rangle\sigma_{il,mn} - \frac{1}{2}\sum_{imn}\langle ml|V[\rho]|ni\rangle\sigma_{ki,mn}. \tag{B14}$$

Equation (B13) appears as an inhomogeneous HF equation, the right-hand side $G(\sigma)$ being an antisymmetric matrix depending only on the two-body correlation matrix σ. This equation reduces to the usual HF condition, when σ is taken to be zero.

APPENDIX C: PROTON-NEUTRON SPLITTING OF THE MIXING COEFFICIENTS

In this Appendix, one assumes that the correlated wave function $|\Psi\rangle$ is particular in such a way that the residual proton-neutron interaction part of $\hat{H}$ deduced from Wick's theorem gives no contribution. This is the case for the correlated wave function used in the pairing application of Sec. III. Then, let us define the restricted Hamiltonian $\mathcal{H}_{\text{restr.}}$ containing only the terms that give a contribution with respect to the correlated wave function that has been chosen. It can always be written as the sum of a proton and a neutron contribution:

$$\hat{\mathcal{H}}_{\text{restr.}} = \hat{\mathcal{H}}^\pi + \hat{\mathcal{H}}^\nu. \tag{C1}$$

In this case, Eq. (8) is equivalent to

$$\sum_{\alpha'_\pi}\langle\phi_{\alpha_\pi}|\hat{\mathcal{H}}^\pi|\phi_{\alpha'_\pi}\rangle A_{\alpha'_\pi\alpha_\nu} + \sum_{\alpha'_\nu}\langle\phi_{\alpha_\nu}|\hat{\mathcal{H}}^\nu|\phi_{\alpha'_\nu}\rangle A_{\alpha_\pi\alpha'_\nu} = E A_{\alpha_\pi\alpha_\nu}. \tag{C2}$$

Since the matrices associated with $\hat{\mathcal{H}}^\pi$ and $\hat{\mathcal{H}}^\nu$ are Hermitians, they can be diagonalized using unitary matrices U^π and U^ν:

$$\sum_{\alpha'_\nu}\hat{\mathcal{H}}^\nu_{\alpha_\nu\alpha'_\nu}U^\nu_{\alpha'_\nu,j} = U^\nu_{\alpha_\nu,j}E^\nu_j, \tag{C3}$$

$$\sum_{\alpha'_\pi}\hat{\mathcal{H}}^\pi_{\alpha_\pi\alpha'_\pi}U^\pi_{\alpha'_\pi,k} = U^\pi_{\alpha_\pi,k}E^\pi_k. \tag{C4}$$

A consequence of Eq. (C3) is

$$\sum_{\alpha_\nu}U^{\nu*}_{\alpha_\nu,j}\hat{\mathcal{H}}^\nu_{\alpha_\nu\alpha'_\nu} = U^{\nu*}_{\alpha'_\nu,j}E^\nu_j. \tag{C5}$$

Applying $\sum_\alpha U^{\nu*}_{\alpha_\nu,j}$ to Eq. (C2) gives

$$\sum_{\alpha'_\pi}\hat{\mathcal{H}}^\pi_{\alpha_\pi\alpha'_\pi}\left(\sum_{\alpha_\nu}U^{\nu*}_{\alpha_\nu,j}A_{\alpha'_\pi\alpha'_\nu}\right) = \left(E - E^\nu_j\right)\left(\sum_{\alpha_\nu}U^{\nu*}_{\alpha_\nu,j}A_{\alpha_\pi\alpha_\nu}\right). \tag{C6}$$

By comparing Eq. (C6) with Eq. (C4), one sees that if the mixing coefficients A and the total energy E are solutions of Eq. (C2), then the quantities $\sum_\alpha U^{\nu*}_{\alpha_\nu,j}A_{\alpha'_\pi\alpha'_\nu}$, should be proportional to one of the $U^\pi_{\alpha'_\pi,k}$:

$$\sum_{\alpha'_\nu}U^{\nu*}_{\alpha'_\nu,j}A_{\alpha'_\pi\alpha'_\nu} = \xi_{jk}U^\pi_{\alpha'_\pi,k}, \tag{C7}$$

where ξ_{jk} is a complex phase, and (C6) shows that

$$E = E^\pi_k + E^\nu_j. \tag{C8}$$

Using Eq. (C7),

$$A_{\alpha'_\pi\alpha'_\nu} = \sum_j U^\nu_{\alpha'_\nu,j}\xi_{jk}U^\pi_{\alpha'_\pi,k} = C^\pi_{\alpha'_\nu}U^\pi_{\alpha'_\pi,k}. \tag{C9}$$

Therefore $A_{\alpha'_\pi\alpha'_\nu}$, solution of Eq. (C2) with the eigenvalue $E = E^\pi_k + E^\nu_j$, is proportional to $U^\pi_{\alpha'_\pi,k}$.

In the same way, by exchanging proton and neutron indices, one shows that $A_{\alpha'_\pi\alpha'_\nu} = C^\nu_{\alpha'_\pi}U^\nu_{\alpha'_\nu,j}$ is an eigenvector of Eq. (C2) with the eigenvalue $E = E^\pi_k + E^\nu_j$. Then, $C^\pi_{\alpha'_\nu}$ is necessarily proportional to $U^\nu_{\alpha'_\nu,j}$. Taking into account the condition $\sum_\alpha |A_{\alpha_\pi\alpha_\nu}|^2 = 1$, one finally obtains

$$A_{\alpha_\pi\alpha_\nu} = U^\pi_{\alpha_\pi,k}U^\nu_{\alpha_\nu,j}. \tag{C10}$$

Consequently, with the form (C1) $\hat{\mathcal{H}}_{\text{restr.}}$, the mixing coefficients $A_{\alpha_\pi\alpha_\nu}$ are products of a neutron and a proton contribution.

[1] P. Ring and P. Schuck, *The Nuclear Many-Body Problem* (Springer-Verlag, Berlin, 1980).

[2] C. Froese-Fischer, Comput. Phys. Commun. **1**, 151 (1969); J. C. Morrison and C. F. Fischer, Phys. Rev. A**35**, 2429 (1987).

[3] D. L. Yeager and P. Jorgensen, J. Chem. Phys. **71**, 2 (1979); H. J. Werner and W. Meyer, *ibid*. **74**, 10 (1981).

[4] D. Vautherin and D. M. Brink, Phys. Rev. C **5**, 626 (1972); Y. M. Engel, D. M. Brink, K. Goeke, S. J. Krieger, and D. Vautherin, Nucl. Phys. **A249**, 215 (1975).

[5] E. Chabanat, P. Bonche, P. Haensel, J. Meyer, and R. Schaeffer, Nucl. Phys. **A627**, 710 (1997); **A635**, 231 (1998).
[6] J. Dechargé and D. Gogny, Phys. Rev. C **21**, 1568 (1980).
[7] J. Dobaczewski and W. Nazarewicz, Phys. Rev. C **47**, 2418 (1993); P. Magierski, S. Cwiok, J. Dobaczewski, and W. Nazarewicz, *ibid*. **48**, 1686 (1993).
[8] T. R. Rodriguez, J. L. Egido, and L. M. Robledo, Phys. Rev. C **72**, 064303 (2005).
[9] J. L. Egido and P. Ring, Nucl. Phys. **A383**, 189 (1982); **A388**, 19 (1982).
[10] J. A. Sheikh and P. Ring, Nucl. Phys. **A665**, 71 (2000).
[11] M. Anguino, J. L. Egido, and L. M. Robledo, Nucl. Phys. **A696**, 467 (2001); Phys. Lett. **B545**, 62 (2002).
[12] M. V. Stoitsov, J. Dobaczewski, R. Kirchner, W. Nazarewicz, and J. Terasaki, Phys. Rev. C **76**, 014308 (2007).
[13] P. H. Heenen, A. Valor, M. Bender, P. Bonche, and H. Flocard, Eur. Phys. J. A **11**, 393 (2001).
[14] E. Caurier *et al*., Rev. Mod. Phys. **77**, 427 (2005).
[15] T. Otsuka *et al*., Prog. Part. Nucl. Phys. **47**, 319 (2001).
[16] N. Pillet, N. Sandulescu, N. V. Giai, and J.-F. Berger, Phys. Rev. C **71**, 044306 (2005).
[17] N. Pillet, P. Quentin, and J. Libert, Nucl. Phys. **A697**, 141 (2002).
[18] P. Quentin, H. Laftchiev, D. Samsoen, I. N. Mikhailov, and J. Libert, Nucl. Phys. **A734**, 477 (2004); K. Sieja, T. L. Ha, P. Quentin, and A. Baran, Int. J. Mod. Phys. E **16**, 289 (2007); L. Bonneau, P. Quentin, and K. Sieja, Phys. Rev. C **76**, 014304 (2007).
[19] B. A. Brown and W. A. Richter, Phys. Rev. C **58**, 2099 (1998).
[20] H. Molique and J. Dudek, Phys. Rev. C **56**, 1795 (1997) and references therein.
[21] J. P. Blaizot and D. Gogny, Nucl. Phys. **A284**, 429 (1977).
[22] D. Gogny and R. Padjen, Nucl. Phys. **A293**, 365 (1977).
[23] S. Péru, J.-F. Berger, and P.-F. Bortignon, Eur. Phys. J. A **26**, 25 (2005).
[24] S. Péru, H. Goutte, and J.-F. Berger, Nucl. Phys. **A788**, 44c (2007).
[25] J. W. Negele, Phys. Rev. C **1**, 1260 (1970).
[26] R. R Whitehead, A. Watt, B. J. Cole, and I. Morrison, *Advances in Nuclear Physics*, Vol. 9 (Plenum Press, New York, 1977).
[27] B. D. Day, Rev. Mod. Phys., **39**, 719 (1967).
[28] R. W. Richardson and N. Sherman, Nucl. Phys. **A52**, 221 (1964); **A52**, 253 (1964); R. W. Richardson, Phys. Rev. **141**, 949 (1966).
[29] J.-F. Berger, M. Girod, and D. Gogny, Comput. Phys. Commun. **63**, 365 (1991).
[30] E. Caurier, G. Martinez-Pinedo, F. Nowacki, A. Poves, J. Retamosa, and A. P. Zuker, Phys. Rev. C **59**, 2033 (1999).
[31] M. Girod and B. Grammaticos, Phys. Rev. C **27**, 2317 (1983).
[32] A. Bulgac and V. R. Shaginyan, Phys. Lett. **B469**, 1 (1999).
[33] A. Trzcińska, J. Jastrzebski, P. Lubinski, F. J. Hartmann, R. Schmidt, T. von Egidy, and B. Klos, Phys. Rev. Lett. **87**, 082501 (2001).
[34] A. Krasznahorkay *et al*., Nucl. Phys. **A731**, 224 (2004); A. Krasznahorkay *et al*., Phys. Rev. Lett. **82**, 3216 (1999).
[35] G. Fricke *et al*., At. Data Nucl. Data Tables **60**, 177 (1995).
[36] S. Terashima *et al*., Phys. Rev. C **77**, 024317 (2008).
[37] F. Le Blanc *et al*., Phys. Rev. C **72**, 034305 (2005).
[38] C. Piller *et al*., Phys. Rev. C **42**, 182 (1990).
[39] I. Angeli, At. Data Nucl. Data Tables **87**, 185 (2004).
[40] M. Anselment *et al*., Phys. Rev. C **34**, 1052 (1986).
[41] J. Blanchot, Nucl. Data Sheets **92**, 455 (2001); **97**, 593 (2002); K. Kitao, Y. Tendow, and A. Hashizume, *ibid*. **96**, 241 (2002).
[42] J. Bron *et al*., Nucl. Phys. **A318**, 335 (1979); A. Backlin *et al*., *ibid.* **A351**, 490 (1981).
[43] F. Andreozzi *et al*., Z. Phys. A **354**, 253 (1996); F. Andreozzi, A. Covello, A. Gargano, and A. Porrino, Phys. Rev. C **41**, 250 (1990); **45**, 2008 (1992).